Results in Engineering 27 (2025) 105845

Contents lists available at ScienceDirect

Results in Engineering

journal homepage: www.sciencedirect.com/journal/results-in-engineering

Research paper

A low frequency seismic triboelectric energy nano-generator used in slow and higher ground motion

José Sánchez del Río [a,b,c,*], Antonio Vázquez-López [b,d], Alba López Laguna [a], Martin Andolfi [a], Rafael Cascón [a], Francisco Santos Olalla [a], Sofía Paramio [a], Yolanda Ballesteros [e], Carlos Cruz [f], Vanesa Martínez [b], José Luis Jiménez [b], Xiang Ao [b], De-Yi Wang [b,*]

[a] Universidad Politécnica de Madrid (UPM), E.T.S. de Ingeniería y Diseño Industrial, C/ Ronda de Valencia 3, 28012, Madrid, Spain
[b] IMDEA Materials Institute, C/Eric Kandel, 2, Getafe, Madrid 28906, Spain
[c] Mechanical Engineering Department, Universidad Pontificia Comillas, Alberto Aguilera 25, 28015, Madrid, Spain
[d] Materials Science and Engineering Area, Escuela Superior de Ciencias Experimentales y Tecnología, University Rey Juan Carlos, Tulipán Street, 28933 Móstoles, Madrid, Spain
[e] Institute for Research in Technology / Mechanical Engineering Dept., Universidad Pontificia Comillas, Alberto Aguilera, 25, 28015 Madrid, Spain
[f] University of Alcala, Department of Electronics, Alcala de Henares, 28871, Madrid, Spain

ARTICLE INFO

Keywords:
Triboelectric energy generators
Seismic devices
Early detection alarm systems
LoRA
Slow ground motion
SLOW-SEISTENG

ABSTRACT

Today sees a need for low-cost detectors able to measure slow ground motion in a broad range of low frequencies. In this sense, the use of triboelectric nanogenerators (TENGS) has been recently suggested, motivated by their low cost and simple design. In this work the use of a TENG for low-frequency detection is explored. This system is based on low-cost polydimethylsiloxane (PDMS)/polyvinyl acetate (PVA) self-power triboelectric energy nano-generator modified single wall carbon nanohorns (SWCNHs). Minimum traction and compression forces of 35 N at minimum velocities of 10 mm/min for elongations up to 4 mm could be detected, without any limit regarding the duration of the excitation signals generated. Relative motion of this system and its parts related to the ground was studied and allowed determining its displacement, velocity and acceleration by following the force damped oscillation model. The effect of electrical induction when inertial mass was either moving to or away from the TENG could be detected, even before contact. A high agreement of the TENG signals generated for frequencies lower than 5 Hz with the external excitation frequency was achieved, corroborating the goodness of the SLOW-SEISTENG when measuring low frequency signals. Lastly, an application as a remote alarm sensor operating with LoRA and Wi-Fi protocols was designed meaning that SLOW-SEISTENG could work as an Early Detection Alarm System (EDAS).

1. Introduction

Currently, there is not any low-cost technology available that is able to measure low and high frequencies, and slow and fast oscillating signals, at the same time[1–3]. Indeed, the creation of such technology remains one of the main challenges that researchers in electronics and communication engineering are seeking with urgency[4,5]. Development of novel sensors associated with this fast-slow motion technology [6] and accompanied by high-resolution data acquisition systems will have a significant impact on our society.

Regarding slow-motion detection, there are few sensor systems of relevance (especially when placed in the ground). In the field of geophysics, slow-motion detection devices such as broadband seismometers and continuous global positioning systems (GPSs)[7–9] allow prediction and mitigation of the severe effects of subsequent faster ones with high frequencies, conversely to slow ones[10] characterized by depletion. In addition, due to bandwidth limitations, as there is not any low-cost geophysical instrument able to observe the full range of slow slips present in ground motions, new quantifications are needed to connect them with faster ones inside a broad spectrum of transient events, thus increasing the possibility that slow slip episodes behave much like ordinary earthquakes[11]. Recently, a triboelectric energy nanogenerator (TENG) called ‘smart maracas’ [12] has opened the door for cost-effective earthquake monitoring solutions. Based on a Falcon

* Corresponding authors.
E-mail addresses: jose.sanchezdelrio@upm.es (J. Sánchez del Río), deyi.wang@imdea.org (D.-Y. Wang).

https://doi.org/10.1016/j.rineng.2025.105845
Received 18 February 2025; Received in revised form 26 April 2025; Accepted 17 June 2025
Available online 18 June 2025
2590-1230/© 2025 The Authors. Published by Elsevier B.V. This is an open access article under the CC BY-NC license (http://creativecommons.org/licenses/by-nc/4.0/).

tube structured filled with plasma-treated surface roughened PTFE balls that interact with an aluminum-coated inner wall, this TENG has been able to response to simulated seismic forces generating a voltage with a significantly high linear correlation coefficient ($R^2 = 0.9989$) with the seismic acceleration.

Although previously tested for high frequency and fast motion[13, 14], only a few TENGs related to slow-motion detection can be found in the published literature. The LV-TENG [15] described by Xiu Xiao et al. precise low-frequency vibration sensing capabilities spanning from 0.1 Hz to 5.0 Hz, crucial for structural health monitoring (SHM) in marine engineering. Employing a cantilever-beam-structured design, it can combine high precision vibration monitoring with micro-energy capture. Chaoran Liu et al. [16] explored the efficient harvesting of ultralow frequency mechanical energy using TENGs, through theoretical modeling and experimentation. Authors underscore the importance of minimizing contact-release time to enhance harvesting efficiency across a wide range of frequencies. I. Mehamud et al. introduced a non-contact-type TENG [17] in order to enhance its durability and anti-wear capability, crucial for machine condition monitoring. Through innovative design featuring permanent magnets and rolling-balls, the TENG facilitates efficient harvesting of low-frequency vibration energy. Regarding blue energy generation and slow motion, a liquid-–solid-contact triboelectric nanogenerator (LS TENG) was fabricated [18] to enhance the friction and magnify energy generation, when compared with the solid–solid-contact TENG with the same area. The buoy-like LS TENG can harvest energy from different types of low-frequency vibration (including up–down, shaking, and rotation movements). Moreover, the outputs of the LS TENGs network can reach 290 μA, 16 725 nC, and 300 V, and the LS TENGs network can directly power hundreds of LEDs and drive a radio frequency emitter to form a self-powered wireless save our souls (SOS) system for ocean emergencies. This work renders an innovative and effective approach toward

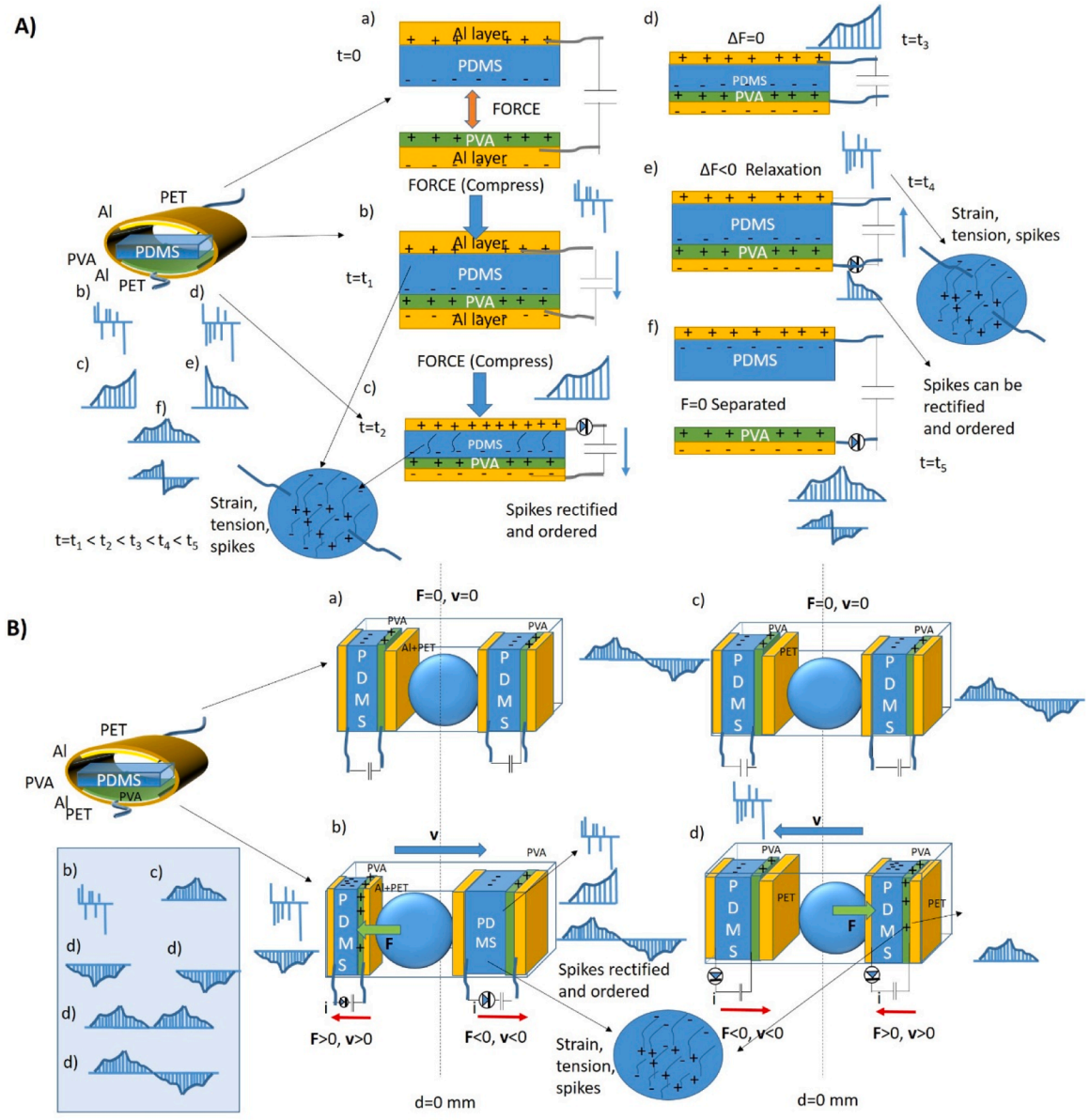

Fig. 1. A) TENG slow-motion detection and waveform generated: a) When positive and negative layers begin to get close one each other by a compression force without being in contact (there is only induction). b) When layers are first in contact. c) When layers begin to be compressed. d) When layers are not supporting any external force and they begin to experience relaxation. e) When layers are recovering the normal position. f) When layers are separated. B) TENG slow-motion detection and waveform generated for the whole seismic sensor: a) Forde F=0 and velocity v=0, the sensor is static; b) the sensor moves to the right; c) again, the ground does not move; d) when the ground or vibrating table moves to the left.

large-scale blue energy harvesting and applications.

Despite the high amount of theoretical models that explain contact and sliding TENG modes working principles[19–23], there is little published research focused on triboelectric energy nanogeneration at slow velocities (slow motion), apart from the above mentioned. A successful approach for the modelization of low (<5 Hz) [24] and ultra-low frequencies (< 1 Hz)[25] was explained by Yunlong Zi et al. and by Chaoran Liu et al. respectively. In the first article, it was demonstrated the high performance of the TENGs for low frequency (typically 0.1−3 Hz) the same as their high performance to drive an electronic circuit for low voltage signals (0.1 – 4 V) and their high output voltage values independent of the frequency. In the second one, a theoretical model of the TENG based on the dielectric-to-dielectric contact-mode is proposed and explains the influence of ultralow frequency mechanical energy with different vibration waveforms.

In addition, some questions are still unsolved regarding the random output voltage generation mechanism measured in such slow motion as when the TENG is operating in its limit of sensitivity. It is M. Willatzen in [26] who really well explains this dynamic behavior of the strain inside the TENG layers, the velocity of the pressure waves and the electrical field, displacement vector and voltage generated inside the material. In some cases, electrical losses in the dielectric avoid electrons recombining with the opposite charge carriers diminishing the triboelectric voltage amplitude. For this reason, these electrical losses, quantified by the dielectric factor loss, should be small and a minimum of force and velocity of the triboelectric layers is needed to have privilege conduction channels along which the accumulated charge will be transmitted and, as a result, collected by either positive or negative electrodes, depending on its sign, and detected by the data acquisition (DAQ) system. The working principle of SLOW-SEISTENG is described in Fig. 1 and in the **section S1**: first, no signal is observed when there is no vibration in the TENG (Fig. 1 a)). Secondly, under compression, some spikes due to the material strain and microstructural stress supported are generated (Fig. 1 A b)). In some cases, a rectifier is used in order to rectify the signals and the spikes can be ordered with the purpose of obtaining a conventional TENG pulse by joining the different maxima (Fig. 1 A c)). After, the TENG is under compression and remains static meaning that there is not any output signal generated (Fig. 1 A d)). Then, relaxation of the layers is produced and again, some spikes due to the stress release are detected (Fig. 1 A e)). Due to the rectifier operation, negative spikes are made positive again, inverted an ordering process starts, conforming the negative part of the pulse according to the standard output response of a TENG in the relaxation mode (Fig. 1 A f)). Another possibility of ordering the spikes is keeping them positive during the relaxation stage and including them after the voltage output obtained during compression. Furthermore, a similar process is followed by SLOW-SEISTENG when an inertial mass moving along the floor of a prismatic box exerts a compression force against the TENG (Fig. 1 B).

In addition, a mixture of slow and fast events could be measured which is extensively explained in the supporting information (see section **S2** and **Fig. S19–21),** specially **Fig. S21** that represents the real seismic sensor setup. The method followed to obtain whole pulses with such a low amount of energy generated as explained above can be performed directly by a software embedded in a processing unit coupled to the sensor under operation or in the cloud when signals have been transmitted remotely.

A similar setup was described by Chuncai Shan[27] et al. In this paper, a versatile blue energy triboelectric nanogenerator (VBE-TENG) made of several rolling balls that impact against contact-separation TENGs (CS-TENG), and sliding ones (S-TENG), all kept inside a big plastic prism box, is shown. Neither velocities of 10 mm/min nor forces of 30 N for long times of contact between triboelectric layers may be achieved with the VBE-TENG. Furthermore, with the system proposed, the induction effect was analyzed and vibration in the Z-axis could be measured by covering the prism box with a rectangular plastic lid, with a TENG glued to it and with an inertial mass on the TENG, as reported elsewhere[28]. Another difference from Chuncai's work is that in the present study can determine the displacement, contact velocity and acceleration for the mass with respect to the box according to the theory of the dumping harmonic model. In addition, in the prototype proposed, TENG signals could be Wi-Fi transmitted to be monitored via http on the Internet with frequency data rates up to dozens of kHz. Furthermore, acceleration and velocity were calibrated for fast and slower events by using the piezoelectric sensor D220-A4BR and the PDMS-based TENG.

Several published papers focused on the ultra-wide range vibration in the vertical and horizontal direction can be consulted in the literature. As reported above, C. Shan et Al[27]. designed a prototype with the capability of detecting frequencies in the range from 1 Hz to 5 Hz in the (X,Y,Z) direction. However, slow motion (low velocities and frequencies f<1 Hz) and fast events (f>10 Hz) could not be measured, with it being difficult to distinguish motion produced in the X and Y directions from the Z one. Shi Q. et al [29]. fabricated a TENG-Ball designed to function as a self-powered multi-axis acceleration sensor. The TENG-Ball shows multi-axis sensing capability that exhibits great potential for various complex motion monitoring. Although for high accelerations the TENG-Ball is very useful, it seems difficult for the TENG-ball to generate voltage under slow motion. Furthermore, there is saturation in the acceleration for the X and Y directions when the ball is turning around. J. Sánchez del Río et al. [28], proposed a TENG seismic sensor able to detect seismic motion in the Z direction. The main concern of this prototype is that it cannot measure in the X and Y axis. This setup is complementary to the one presented in this work and can be easily integrated, producing a 3D TENG seismic system (the Y direction is symmetric to the X direction and is 90º turned related to the sets-up in the X direction).

A self-powered -triboelectric–electromagnetic hybrid nanogenerator has been developed by Hongxin Hong et al. [30] and harvests energy from water waves with a wide frequency and different directions. The seesaw-structured spherical buoy was used to drive a global positioning system (GPS) module for dynamic sea surface real-time wireless positioning. However, again, neither slow motion nor induction could be detected with this device. Qingyun Ying et al. [31] propose an omni-directional multi-track spherical structure TENG (OMS-TENG) with eight fan type TENGs (FTENGs) per layer for harvesting low-frequency ocean energy. The OMS-TENG output performance remains essentially stable as the wave direction shifts from 0° to 360°with a translation frequency of 1 Hz and translation displacement of 40 mm thanks to the eight different directions of FTENG inside OMS-TENG. The main drawbacks are its use for higher frequencies resulting in reduced and disordered output performance, and that slow motion not being measured in this system as it does not operate with an initial preload.

In this work, the seismic sensor presented is named SLOW-SEISTENG and it is based on the triboelectric and strain effect, with an inertial mass sliding on the base of a polylactic acid (PLA) 3D printed box that impacts on it. Velocities in the range between 10 and 100 mm/min and forces up to 450 N with frequencies lower than 5 Hz in an isolated compressing setup to test the limits of the slow movement is shown as well as the limitation of the thickness of the PDMS layer, that is very relevant for the device sensitivity. An explanation of the slow-motion phenomenon detected by TENGs is shown experimentally and signals obtained by induction when the inertial mass is charged and is approaching the TENG (without contact) can be observed by the signals generated, satisfying theories based on Maxwell equations that explain working principle of TENGs with or without contact[22]. Furthermore, the modelling of this slow motion by considering the TENG as a plane-parallel layer capacitor separated a variable distance and its agreement with the results obtained when the same design is introduced in COMSOL, is presented. The relative motion of SLOW-SEISTENG related to the ground is calculated with the vibration damping theory and as a result, its displacement, velocity and acceleration is calculated. To finish, an alarm sensor designed with a wireless communication signal such as with LoRa and Wi-Fi protocols is used. This application

makes SLOW-SEISTENG an excellent early detection alarm system that can be set-up in any place inside/outside the ground with the aim of mitigating and prevent the population of possible catastrophic events.

2. Materials and methods

2.1. Fabrication of the TENG materials

The TENG used had two layers: one of polyvinyl-alcohol (PVA), and one of polydimethylsiloxane (PDMS). In addition, Al paper was included to fix the electrodes. Details regarding fabrication and materials employed in Al-paper:PDMS-Al TENG can be obtained elsewhere[13, 32]. Different thicknesses in the PDMS layer could be fabricated (1, 2 and 4 mm). The whole size of each TENG is 40 mm × 37 mm, while the active area (the size of PVA layer and PDMS films) is 30 mm × 35 mm during the electrode electric connection in the tests. The PDMS layer thickness used for sensing is of 4 mm.

Furthermore, to obtain modified PVA and modified PDMS, a Single Wall Carbon Nanohorns (SWCNH) suspension was slowly added into the aforementioned PVA solution (10 g, 10 %) and stirred for 1 h. Finally, the two-component (PVA/SWCNH) solution was poured onto the surface of the glass bottom plate of the scraper coating testing machine (TBJ-B1, China) to obtain the SWCNH modified PVA film (m-PVA) with a thickness of 0.2∼0.3 mm. The same process was performed with the PDMS film. After degassing under vacuum for approximately 30 min, the obtained PDMS/SWCNHs mixture was poured into a polytetrafluoroethylene mold and cured at 100 °C for 35 min to obtain the SWCNHs-modified PDMS film (m-PDMS) with thicknesses of 1 mm, 2 mm and 4 mm.

2.2. TENG voltage signals at slow traction/compression experiments

All measurements have been performed at room temperature and humidity conditions. Two different electromechanical testing machines Figure S1 b) and e) fabricated by Ibertest and placed at the ICAI School of Engineering at the Universidad Pontificia de Comillas with a load cell of 500 N were used in slow-motion mode with the 4 mm thick PDMS-based TENG. The range of forces chosen ranges from 30 N to 470 N at speeds of 25 to 500 mm/min.

Another compression electromechanical machine fabricated by Servosis (see Figure S1 a) and Figure S1 f)), with a load cell of 2 kN, is placed at the E.T.S. de Ingeniería y Diseño Industrial (Universidad Politécnica de Madrid). The forces chosen ranged from 20 N to 150 N at a speed of 50 mm/min. in order to protect the load cell, a soft sponge (silicon block) was placed between the upper and lower jaw plates of the testing system, resting on the lower one so that the TENG could remain stacked between the upper jaw and the silicon block when thejaw had reached the TENG. This configuration could induce electromotive force in the TENG.

Lastly, a traction/compression hydraulic machine fabricated by INSTROM and placed at the IMDEA Materials Institute (see Figure S1 c) and Figure S1 d)), with a load cell of 500 N, operated at velocities in the range of 25 to 100 mm/min and forces applied varied between 200 N and 400 N for a speed of 50 mm/min. A summary of the mechanical testing machines and utilities is presented in Table 1.

Table 1
Traction/compression electromechanical machines and parameters used according to the test performed.

	ETSIDI Testing machine (SEVOSIS)	IMDEA Materials Testing machine (INSTROM)	ICAI Testing machine (1) (IBERTEST)	ICAI Testing machine (2) (IBERTEST)
Induction	Yes	No	Very small (isolated)	No
Speed	0–50 mm/min	0–100 mm/min	0–50 mm/min	0–500 mm/min
Force	0–150 N	0–500 N	0–500 N	0–500 N

2.3. TENG calibration curves for low and fast events with the piezoelectric sensor D220

A 2-layer piezoelectric actuator and sensor D220-A4BR-1305YB from PIEZO.COM[33] was used to calibrate the TENGs integrated in the seismic prototype. For this, TENG and piezoelectric sensors were crabbed between the jaws of an INSTRON mechanical traction/compression machine which was programmed to move at different velocities (**Figure S1** g) and h)). First, only the piezoelectric sensor was calibrated for velocity and acceleration up to forces of 1 N and jaw elongation of 0.2 mm. Then, for the TENG calibration, the TENG together with the piezoelectric sensor D220 were inserted too between the two jaws but one separated from the other so that force and elongation could be monitored by the INSTRON software while the user was compressing/releasing the TENG-Piezo system with the hand.

2.4. Vibration tables for different frequency impacts

A vibration table from the Matest model C278 (Figure S2 a)) with dimensions of 600 x 400 was used to generate vibrations in the frequency range of 1 to 5 Hz under different displacements of the prism box with the metal sphere inside. Mass (546.7 ± 0.8 g) and radius (50.7±0.1 mm) of this metal sphere was calculated and shown in Section S3 of SI the same as the TENG stiffness (151 ± 10 N/m). In order to measure different TENG impacts caused by the inertial mass, either only one or two prism boxes with two cylinders inside, one for each, were screwed to a Quanser Shake vibration table owned by ICAI, that was programmed to vibrate in the frequency range of at 1 – 5 Hz (Figure S2 b).

2.5. Data acquisition systems (DAQs)

A Picoscope 2000 oscilloscope (Figure S3 a)), with Picoscope 7 software, was programmed to measure at 200 Msamples/s in intervals of 10 s with the software used to filter the signal up to 1 Hz (low pass filtering) in order to eliminate high-frequency noise. This DAQ was also used to detect induction phenomena produced in the TENGs during traction and compression processes and when measuring different vibration frequencies.

The Agilent Technologies InfiniiVision DSO-X 3012A digital storage oscilloscope was configured to operate with a rate of 20 kSamples/s in a 10-second capture screen. The maximum rate of the oscilloscope is of 100 MHz and 4 GSamples/s. This was only used for measurements performed with the first Ibertest testing machine.

A Conventional ISO-TECH (IDS 6052-U) digital oscilloscope from the ETSIDI and DP2012B Tektronix one from IMDEA Materials were also used to measure TENG signals.

2.6. Measuring the electric current

In order to measure the electric current generated in the TENG, a low-noise current preamplifier, model SR570, from Stanford Research Systems (Figure S3 b)), was used for calculating different sensitivity values depending on the velocity and force applied. The TENG output was connected to the input of the preamplifier; and the preamplifier output to the input of one of the channels of the Piscoscope oscilloscope.

2.7. Software and programs used

A MATLAB program designed by the authors was used to plot a voltage (V) generated signal, force exerted by the jaws on the TENGs and the elongation. It allowed determination of slow oscillations due to electric induction produced by the mechanical testing machine jaws with a similar filter to that used in the Picoscope (low pass filter). This is

known as the moving average function that is dependent on the parameter α which is less than 1. Often α=0.01 was chosen and represents the cut-off frequency used in a standard low pass frequency filter. Furthermore, Python programming language in the Google Collaborate platform was used to simulate the TENG voltage and current generation and COMSOL, the electrical potential distribution.

3. Results

3.1. Calibration of TENG signal response for low velocities

The first step was calibrating the TENG for low velocities and observing the pulse formation and duration. Velocities of 10, 25, 50, 75 and 100 mm/min were programmed in the INSTROM testing machine, producing a compression and traction of the 4 mm thick PDMS-based TENG crabbed by its jaws. Picoscope DAQ was used to detect the voltage generated by the TENGs and a MATLAB program developed by the authors and allowed these signals to be recorded together with the force programmed by the INSTROM software which was applied by the jaws and with elongation in a Z-direction (see video **SV1**). Low band-pass filtering at different cut-off frequencies such as 1 Hz and 10 Hz was implemented in the MATLAB software to analyze low-frequency signals generated by the TENG. Furthermore, low-pass filtering was also used in the Picoscope software and a calibration curve was performed for either raw voltage generated by the TENG or filtered voltage signal obtained with the Picoscope and MATLAB program. In Fig. 2 , raw signals measured at a) v=100 mm/min, b) 75 mm/min, c) 50 mm/min and d) 10 mm/min are shown, with the last one being only for one pulse in order to remark such a long- pulse duration. All are pulses obtained for 450–500 N force applied by the jaws on the sensor and present a pulse time duration of more than five seconds (5.4 s when considering the highest peaks and 20.4 s if considering the ones at the beginning and at the end, shown in Fig. 2 (d)). This time length corresponds to the time the jaws are in contact with the TENG at some velocity. In order to visualize the whole force excitation signal for the same kind of tests, the same Fig. 2 a) – c) is plotted in the **Figure S4** a) – c) but with a change of scale of x0.01 in the force magnitude with the purpose of visualizing the whole force profile.

Furthermore, for a velocity of 10 mm/min, a constructed pulse of 27.4 s of time length is shown in **Figure S4** d) when the lowest V peaks inside the excitation curve are taken in account and about 5.5 s considering only the highest ones which by chance are the ones under the excitation curve. In **Figure S5,** an example of filtered V pulse for 1 Hz cut-off frequencies is shown for (a) 100 mm/min and (b) 10 mm/min where only the contact of the jaws with the TENGs is shown but voltage pulses of the train-wave discriminated. In addition, calibration curves related to filtered and raw voltage at 1 Hz vs. velocity are presented in **Figure S5** (c) and (d) respectively, with all having a jaw force applied to the TENG of 450 N. In the case of filtered signals, the Ibertest machine was used to apply compression and traction forces to the TENG of 450 N at velocities up to 500 mm/min and the DAQ employed was the oscilloscope DSO-X 3012A that measured and stored filtered signals, allowing a calibration curve up to 500 mm/min.

In order to evaluate the TENG response for different forces applied, such forces up to 500 N were applied at the velocity of 50 mm/min. Calibration curves of voltage-force were plotted for raw and filtered voltages respectively and are shown in Fig. 3 (a) and (b). In addition, the time length of the pulses was also evaluated with the purpose of

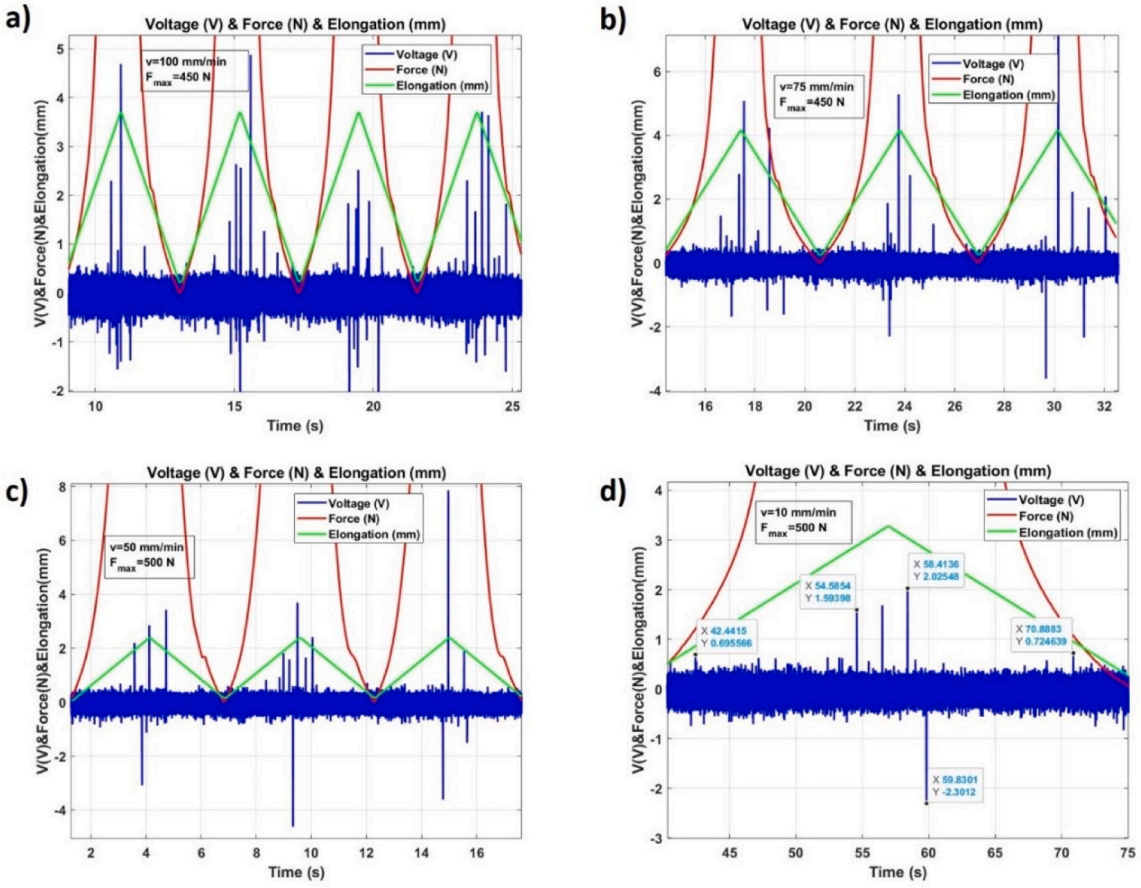

Fig. 2. Raw voltage V generated by the TENG (blue) when compressed and released under a jaw force F (red) and elongation programmed (green) with an electromechanical testing machine for a) v=100 mm/min, b) v=75 mm/min, c) v=50 mm/min and d) v=10 mm/min.

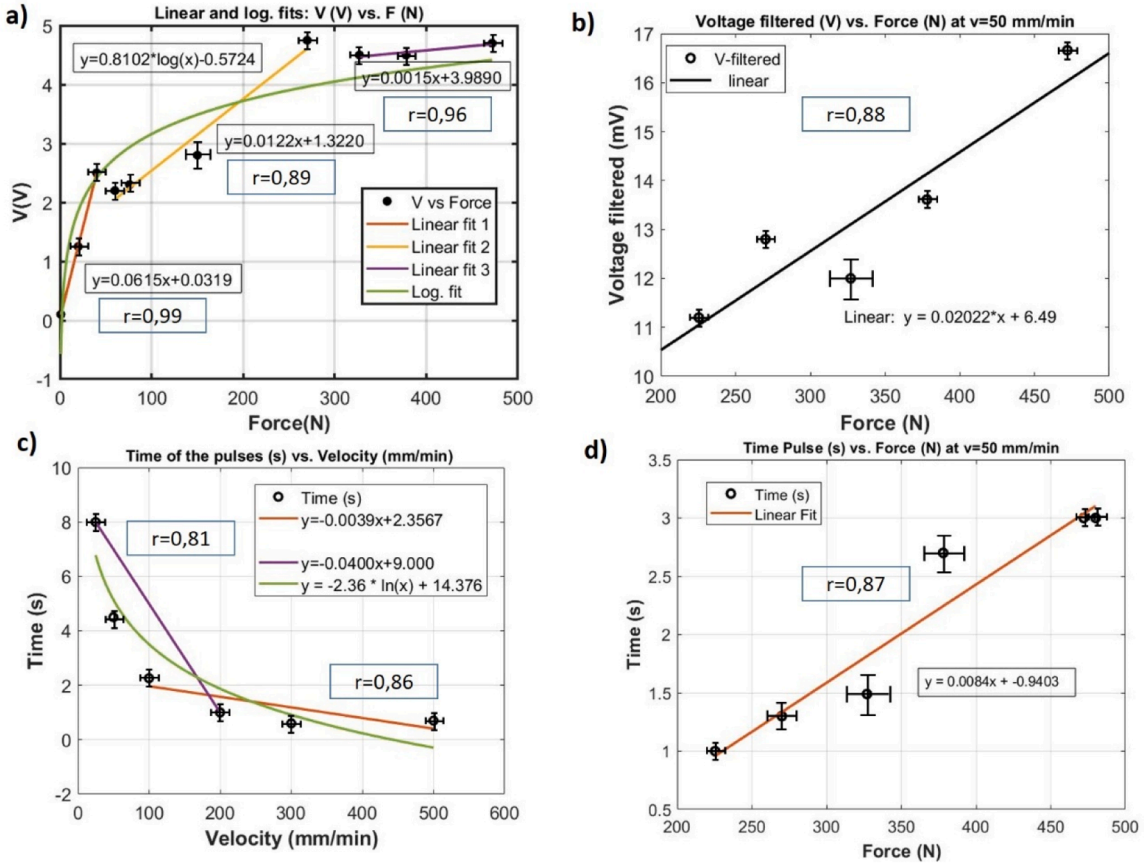

Fig. 3. Calibrations with linear and logarithmic fits of a) raw amplitude V of the pulses vs. Force applied by the jaws, b) low band-pass filtered amplitude V vs. Force applied, c) time length of the raw V pulses vs. Velocity and d) time length of the low band-pass filtered V pulses vs. Force applied.

analyzing the dynamic behavior of the TENG response. It was tested that for the lowest traction/compression velocities where a signal could be still detected (v=10 mm/min), pulse time length was of eight seconds for an applied force of 500 N (see Fig. 3 (d)). This can be also seen in Fig. 3 (c) where time length of the pulses vs. velocity of the jaws and in Fig. 3(d) vs. the force applied are depicted.

In most groups of pulses (vertical lines) there are some higher voltage peaks (V_{peak}) than the mean, with all corresponding to each pulse and monitored too. Calibration curves of peak voltage vs. force and velocity are presented in **Fig. S6** (a) and (b). In addition, a train of pulses for a maximum force applied of F=35 N (F=20 N programmed in the testing machine software, but for inertia of the jaws a maximum force of F=35 N was reached) and a velocity of 50 mm/min is shown in **Fig. S6** (c), although they are not as uniform in shape and amplitude as in higher force and velocity modes. However, some degree of pattern can be perceived and used as valuable data when constructing a calibration curve. During the same experiment, forces up to 500 N for velocities of 10 mm/min were applied and either the force profile or V_{raw} pulses are shown in **Figure S6** (d). As reported in **Figure S6**(d), time of contact length between the TENG and jaws takes place every 30 s.

3.2. Selection of the best TENG thickness triboelectric layers

Different combinations of TENG layers with 1, 2 and 4 mm thick were performed in order to determine the highest efficient transducer of the SLOW-SEISTENG. The highest ones have 4 mm of PDMS thickness and were the mPDMS – PVA-based TENGs for velocity values higher than 40 mm/s and the PDMS-PVA-based (see **Fig. S7**). However, as the PDMS-PVA based TENG is cheaper and easier to fabricate than the mPDMS-PVA one, this material based transducer was the one selected to fabricate the SLOW-SEISTENG seism detector. However, when higher sensitivity is needed, the 4 mm mPDMS-PVA-based TENG is recommended.

Sensor signals obtained from 2 mm PDMS thick TENGs when measuring the same velocity as described in the previous section and with the same experimental procedure were compared with those obtained for 4 mm. In this case, the force applied between jaws was 400 N. It is shown in **Fig. S8** that under these conditions, sensitivity is half when using a TENG with 2 mm thickness, either when registering the highest peaks or the raw signal. With V_{peak} we refer to the highest spikes and with V_{raw} to an average voltage of the pulses detected. The same measurements were carried out with TENGs of 1 mm PDMS layer thick for the same velocities, though in this case the amplitude of the voltage pulses generated was low and, for the slowest velocities, immersed inside the noise. Conversely, it was tested that for high velocities and frequencies, 1 mm thick PDMS based TENGs presented the highest response because only contact between the jaws and the TENG layers was measured.

3.3. Experimental and simulated results of SLOW-SEISTENG under slow motion

According to the electrostatic energy stored and released by the TENG when operating under traction and compression modes, it was possible to determine the electric current generated by the TENG due to the friction between layers. TENG is considered as a planar capacitor with a capacitance C given by the formula: $C = \varepsilon S/d$ with ε the electric permittivity of the PDMS (as that of the PVA is thin, it is considered that TENG layer permittivity is little affected by its contribution), S as the area of the capacitor layers and d as the thickness of the dielectric ma-

terials (PDMS layer of 4 mm thick). According to Niu et al. [34], the basic equation for the contact-mode TENG can be utilized in this paper to calculate its output property. Eq. (1) was solved by the authors using Radau solving method programmed in Python and using Google Collaborate platform to execute the code:

$$R\frac{dQ}{dt} = -\frac{Q}{S\varepsilon_0}(d_0 + x(t)) + \sigma\frac{x(t)}{\varepsilon_0} \tag{1}$$

where R is an arbitrary electrical resistor R, $d_0 = \frac{d_1}{\varepsilon_1} + \frac{d_2}{\varepsilon_2}$, with d_1 is the first (+) triboelectric thickness (PDMS) and d_2 the second (-) (PVA), Q is the amount of transferred charges between the two electrodes, x(t) is the distance between the two triboelectric layers that can be varied under the variation of mechanical force, which it will be considered as harmonic, σ, the surface charge density and ε_0 the absolute dielectric permittivity. The study has taken the cosine moving mode as the expression for x(t) in the following way:

$$x = \frac{-x_{max}}{2}\left(1 - \cos\left(\frac{\pi\vartheta}{x_{max}}t\right)\right) \tag{2}$$

with ϑ the oscillation frequency. Here, x_{max} is the maximum separating distance between layers. For a surface charge density of $8x10^{-6}\ \frac{C}{m^2}$, $x_{max} = 1.8\ mm$, $S = 0.0105\ m^2$, $R = 2x10^9\ ohms$, $d_1 = 4\ mm$ *and* $d_2 = 0.5$ mm, $\varepsilon_1 = 2.5$ *and* $\varepsilon_2 = 2$. Using this expression of x(t), a compression of the tribolayers is produced, being on contact one against each other. As velocity of the triboelectric layers is defined as $v = x_{max}\ \vartheta$, we can calculate the electrical current generated by the TENG for different velocity values making use of this theoretical model described above. Furthermore, TENG electric current was measured with the low noise current amplifier, model SR570, for several traction compression cycles under different velocity values. The results are

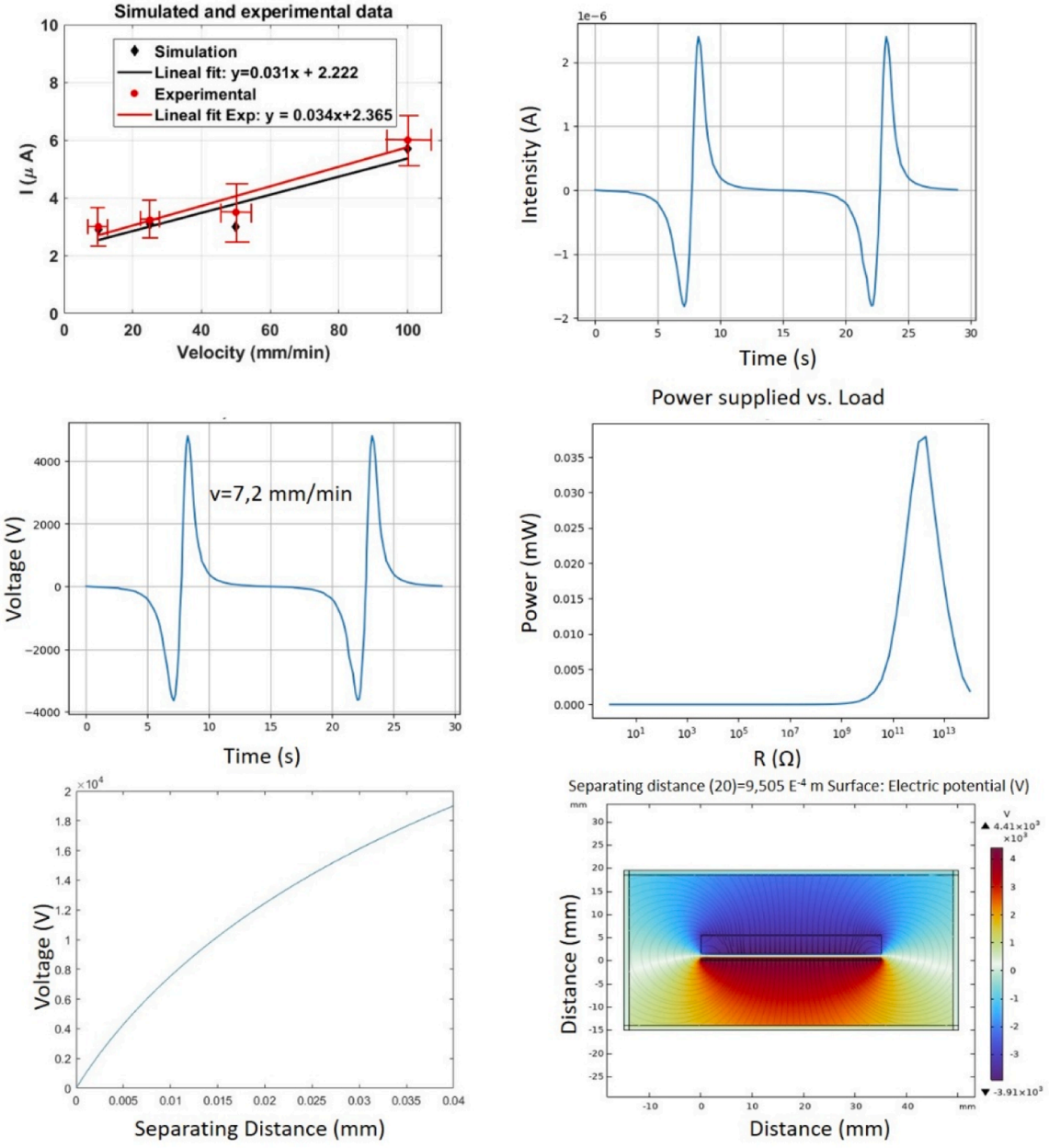

Fig. 4. a) TENG Electric current (simulated with Python in Google Collaborate/directly measured) vs. velocity; b) Pyhton simulated intensity of the pulse waves; c) Python simulated voltage of the pulse waves; d) Python simulated electrical power supplied vs. electrical resistance; e) COMSOL simulated voltage generated by the TENG vs. separating distance; f) COMSOL surface electrical potential for a separating distance between layers of 1 mm.

shown in the calibration curve presented in Fig. 4 (a), where electric current (I_{exp}) is in the same order of magnitude as that calculated from previous formulae and is highly in agreement. In Fig. 4 (b), the current pulse generated by the TENG and simulated in Matlab [35] is shown and the same but with the voltage is presented in Fig. 4 (c). In Fig. 4 (d), electrical power generated by the TENG and dissipated by the optimal electrical resistance with a maximum value of 0.035 mW is shown. In addition, voltage generated by the TENG and the separating distance was simulated with COMSOL[36] and is presented in Fig. 4 (e). Here, the capacitor formed between the triboelectric layers with no external resistor connected (open circuit condition) is variable regarding the separation distance. The relationship between this distance and the potential does not present a linear trend because of the stabilization or equilibrium state reached by the triboelectric charges when the separation distance is maximum. Furthermore, the electrical potential distribution vs. the separating distance was simulated with COMSOL too is shown in Fig. 4 (f). Results obtained with COMSOL present even a high agreement with the ones obtained with Matlab,

3.4. The principle of the TENG pulse formation for slow motion

In order to understand the mechanism of the pulse formation under different force magnitudes (0–500 N) for a velocity of 50 mm/min and provide an explanation of the appearance of certain peaks which can be observed under slow traction and compression forces, maxima voltage for each traction/compression cycles were selected and joined with continuous traces so that waveforms could be obtained for the different force cycles, as shown in **Fig. S9** (v=50 mm/min, 200N<F<400 N). A MATLAB program was used to fit the force pulses generated in each traction/compression cycle to Gaussian functions. Once the program was executed for all the pulses, only a few could be properly fitted for forces below 400 N which meant that only a few such pulses could be formed under these conditions with a recognized pulse shape and after electrostatic energy had been either released or gained under the different mechanic cycles programmed with the mechanical testing machine software. As seen in Fig. 5, when force is 400 N, all pulses are well formed and fitted to Gaussian functions. In addition, pulse voltage vs. velocity of the jaws for repeated tests under a force of F=450 N was plotted in several graphics and shown in **Figu. S10-S12**. It can be seen that for v=10 mm/min only half of the pulses were properly formed. In the case of v=25 mm/min, v= 50 mm/min and v=75 mm/min, 75 % of the pulses were well generated and for v=100 mm/min all the pulses were formed with waveforms fitted to Gaussian functions.

3.5. The effect of the electrical induction in SLOW-SEISTENG

Evidence has been provided of electric current generation without any contact between the external force element and TENG layers[37], although under some degree of restriction. In the experiment, the external force agent corresponds to the traction/compression jaws of the Servosis mechanical testing machine which in this case were electrified for the experiment with a small current of 200 mA, 1 V and 50 Hz due to the connection of an alternating electric power source to the metal case of the machine. In addition, a PLA 3D printed prism box with two TENGs, one glued to the back and the other to the front, were screwed to a V10 shock table which vibrated with the different frequencies programmed in the PA100 amplifier controller. A metal sphere or a cylinder, charged due to friction with the base of the box, slid on the bottom surface and hit the TENG sensors which were compressed by this inertial mass when it was in contact with them. Furthermore, a Quanser

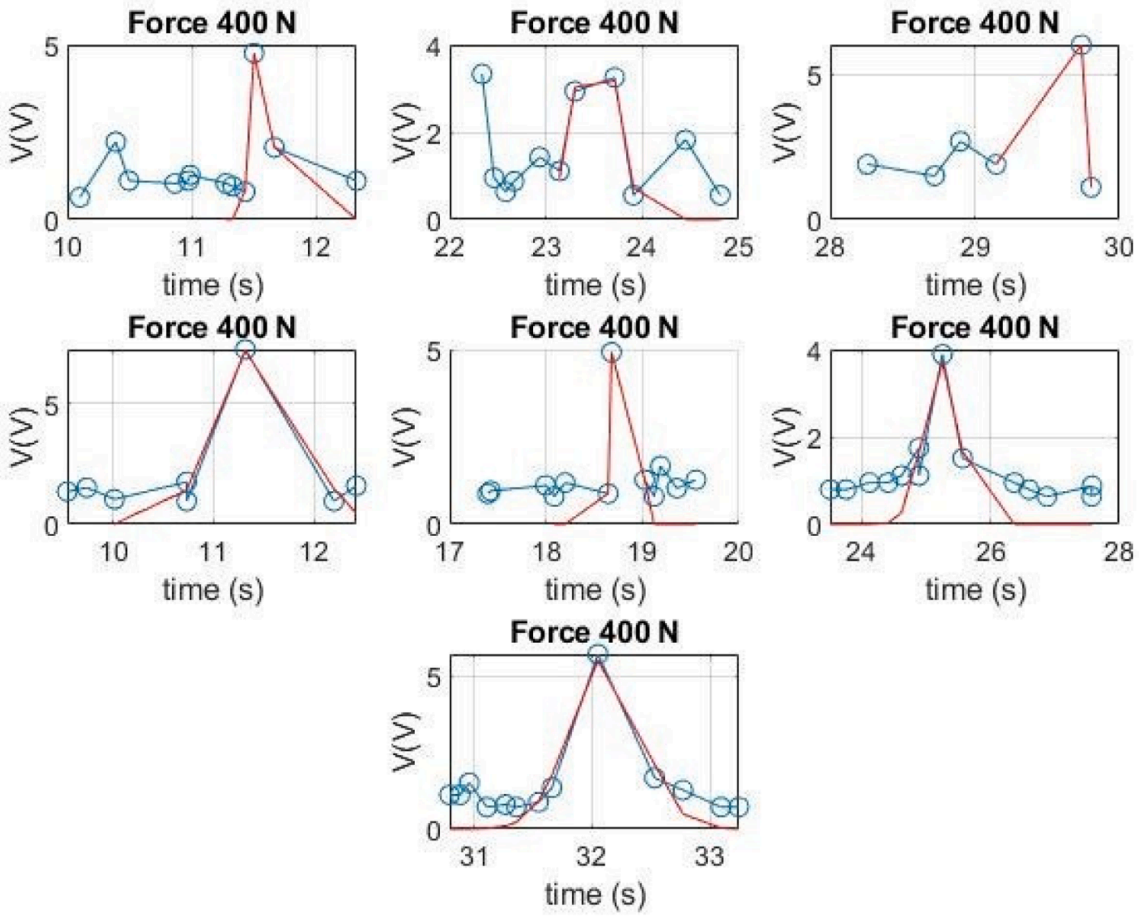

Fig. 5. Representation of the different pulse shapes obtained by joining the V peaks measured for trials with a force of 400 N and with a velocity of 50 mm/min.

vibration table was also used for the same frequencies, elongations and forces.

During the distance run by the inertial mass, a drift signal due to electric induction could be measured as the same as the high pulse generated when impact with the TENGs was produced. This setup was also developed to measure high frequencies due to pure impact of the mass against the TENG. Voltage signals generated by the TENG when the traction/compression mechanic machine operated at 0.2 Hz are presented in Fig. 6 a) in which induction produced by the jaws charged and exerting a maximum force of 70 N may be observed. Once a signal is low band pass filtered with shortcut frequency parameter α of 0.1 %, high peaks corresponding to impacts of the inertial mass with the TENG and after, sinusoidal signals due to induction effect are observed. Raw voltage measured directly from the TENG with the Picoscope DAQ is presented in Fig. 6 c) for a frequency of 0.2 Hz and for an elongation between jaws of 1.7 mm and a force F=25 N when first in contact. In this figure, low oscillations caused by the electromagnetic induction when the jaws were not in contact could be measured. Furthermore, as shown in Fig. 6 b) and d), when a low band-pass filter (of the type simple mobile average (SMA)) with a shortcut frequency parameter α of 0.1 % was implemented, oscillations of 0.2 Hz of frequency were detected, thus proving the effect of the electromagnetic induction during the entire traction/compression cycle (even when the TENG and jaws were not touching).

A comparison between TENG tests with and without impact caused by the inertial mass (electromechanical jaws) is shown in the raw-voltage signals provided in Fig. 7 (a) for F=75 N and b) for F=25 N. Again, the induction signal is observed as a sinusoidal form and contacts between layers are related to the voltage peaks: firstly, a lower and longer signal due to electromagnetic induction when the inertial mass is approaching the TENG; secondly, a peak voltage signal caused by the impact of the inertial mass when the TENG is detected. In the case of F=150 N, the waveform pattern is similar (see Fig. 7c)). In Fig. 7d) a low band-pass filter (SMA) is applied for α=0.001on the previous plot and no impact of the inertial mass and the TENG is observed.

3.6. Calibration of SLOW-SEISTENG in the frequency domain

A vibration table for excitation frequencies in a range from 1 to 5 Hz and displacements from 3 to 15 mm was used, with the sphere inertial mass hitting the TENG. Furthermore, data analysis was performed by using the first (principal) harmonic of the FFT[38–40] frequencies. Voltage generated by the TENG when the inertial mass compressed and released its layers for the frequencies of 1 Hz, 2 Hz, 3 Hz, 4 Hz, 5 Hz and 30 Hz programmed in the shake table is shown in Fig. 8 a)-f).

In addition, these frequencies and the corresponding harmonics obtained by applying the FFT to previous time-domain signals are shown in the spectra presented in Fig. 9 a) - f). A calibration curve of the raw and peak voltage of the first FFT harmonic in the frequency range of 1–5 Hz can be seen in **Fig. S13**.

Here, spectra reveal with more clarity the frequencies transmitted by the table and generated by the TENG with an outstanding response. A frequency of 30 Hz was even detected for the MASTEC vibration table oscillation frequency. In Fig. 10 a) the FFT amplitude (first harmonic) of the voltage generated by the TENG vs. the maximum elongation (amplitude) supported by the shake table is presented. In Fig. 10 (b-f), the voltage of the wave generated by the TENG excited by the shake table vs. contact and table velocities at the frequencies of b) 1 Hz, c) 2

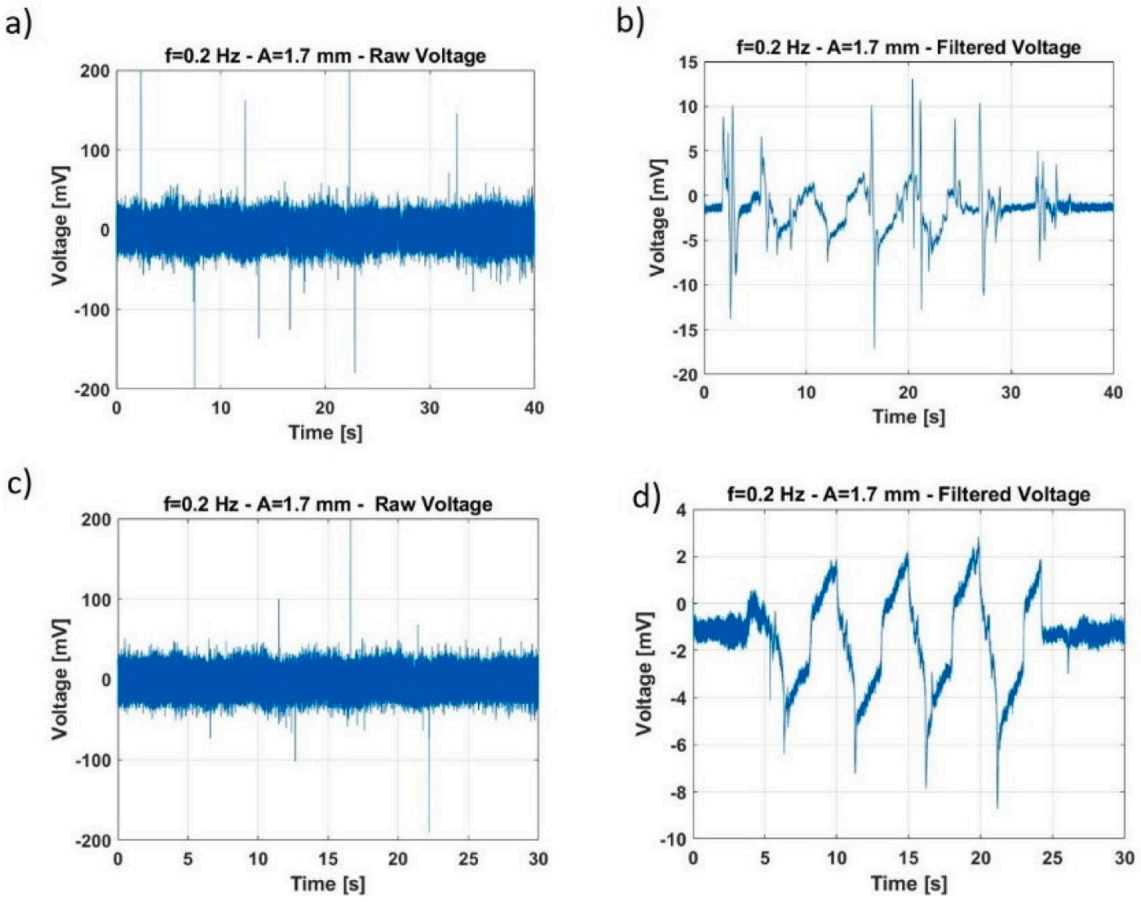

Fig. 6. Filtered signals with α=0.001 as a parameter of low band pass filter. Raw data for tests with an applied force of a) F=70 N and with impact, F=25 N without impact (c) and b), d) both filtered signals respectively in the mechanical testing machine.

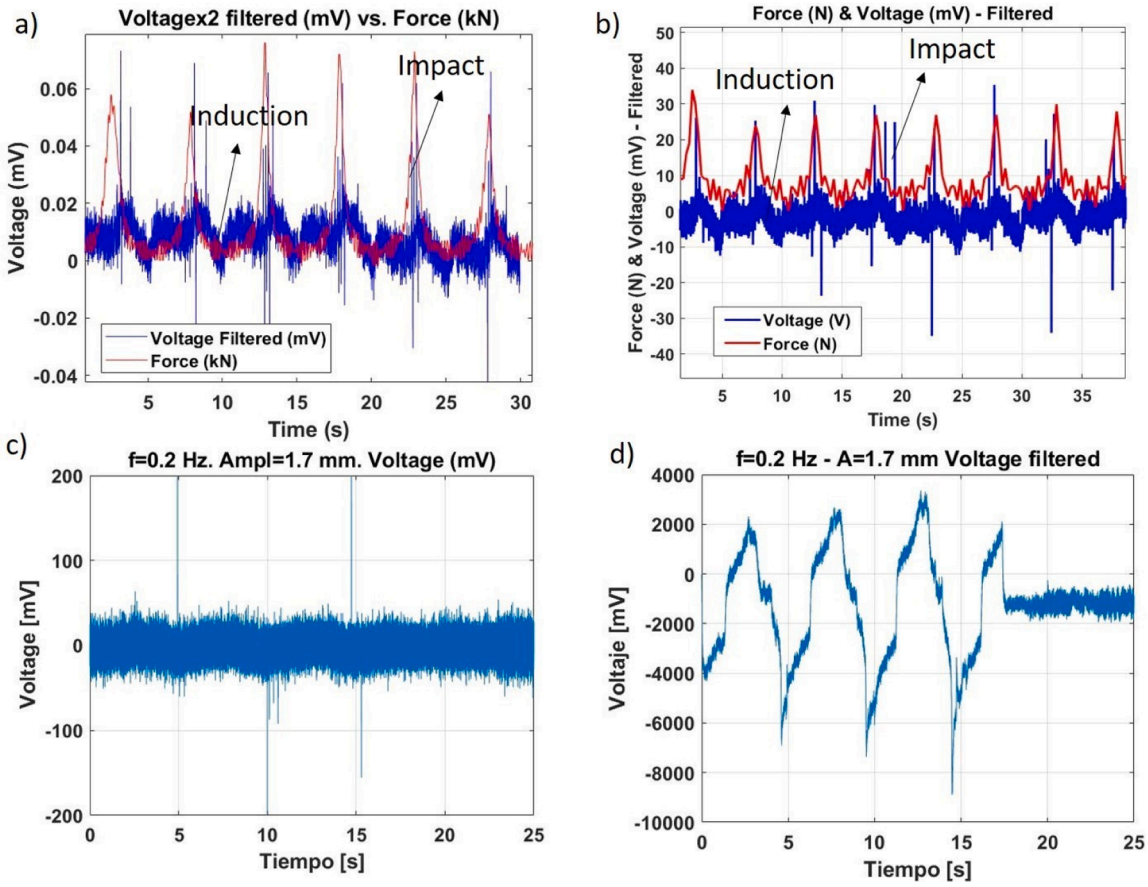

Fig. 7. V signals generated by the TENG under traction/compression forces: a) F=75 N, b) F=25 N. c) Raw voltage signals obtained for f=0.2 Hz, F=150 N and initial separation distance between jaws of 1.7 mm. d) Filtered signal with α=0.001 (0.1 %) low pass filter. All were tested for v= 50 mm/min.

Hz, d) 3 Hz, e) 4 Hz and f) 5 Hz is shown. Contact velocity is defined as the product of the amplitude (A) and the frequency (w) (v=A x w), with both programmed with the MATEST software of the vibration table and demonstrates the velocity at the instant of the contact between the inertial mass and the TENG. Table velocity was calculated by using the forced damped oscillator mathematical model in which a spring is attached to a support (see **section S3**). Here, the spring is the TENG with an elastic constant k which was previously calculated (**see section S4**) and the support is the vertical wall of the 3D printed box.

This model allows determining the displacement, velocity and acceleration supported by the triboelectric sensor under compression and traction forces transmitted by the metal sphere by including the experimental values of the table amplitude and excitation frequency. In addition, a calibration of the acceleration supported by the mass and the voltage generated by the TENG when the metal sphere is in contact with the TENG and inside the 3D printed PLA box can be seen in **Fig. S14**. Again, acceleration was calculated by using the forced-damping oscillation model with amplitude and excitation frequency as input values ($a=A\ w^2$) and voltage obtained from the first harmonic of the FFT (see **Section S3**). As can be seen from the figures, velocity and dispersion are relatively low (r=0.92) for frequencies lower that 5 Hz, however, for f=5 Hz, it is higher (r=0.6) (see Fig. 10 f)) and an improved mechanical setup to measure impacts on the TENGs and obtaining more correlated ground velocity and acceleration values is needed, especially when the mass is rolling on the base of the prism with friction. It is suggested using a frictionless surface (similar to ice) for seismic sensors similar to the ones described here, with a mass sliding on the floor of a prism box and for medium oscillation frequencies (5–7 Hz). With higher frequencies, the mass will remain fixed and for lower ones it will follow the oscillation of the ground. Furthermore, when there was no preload the same set-up with the 3D printed PLA box was maintained and results for frequencies of 1 Hz, 1.5 Hz and 2 Hz were measured and can be seen in Fig. 11 (see also **Fig. S15** for frequencies in the range 3–5 Hz).

3.7. Calibration of the TENG with the piezoelectric sensor D220-A4BR

Accurate D220 piezoelectric sensor voltage responses with outstanding waveforms were obtained for jaw velocities of 0.5, 1, 10 and 40 mm/min for a force of 1 N exerted on the piezoelectric sensor (see **Figures S16** a) and b) and **Figure S17** a)). It was tested that variations of such force for the same velocity did not change the output signal, neither in the waveform nor in the amplitude response. A calibration of the voltage generated by the TENG and the voltage generated by the piezoelectric sensor was performed for the same excitation frequencies resulting in a linear calibration fit (**Figure S16** b)). In addition, a linear calibration curve of the jaw velocity and acceleration (**Figure S17** b)) that are the same as the ones supported by the TENG layers was obtained for the same force supported. In addition, a comparison of the TENG and Piezoelectric response for different velocities and accelerations calculated with previous calibrations is presented in Fig. 12 a) – d) for the same force F=30 N and for the periods of ΔT= 0.1 s (Fig. 12 a) and b)) and ΔT= 1 s (**Figure S16** c) and d)) a high agreement of the signals was obtained.

3.8. Application of SLOW-SEISTENG as an early (Smart) detection alarm system

As a real application of SLOW-SEISTENG, a Wi-Fi and LoRA alarm system was developed in order to operate as an EDAS (Early Detection Alarm System). For this, a DAQ from National Instrument (NI-USB-600)

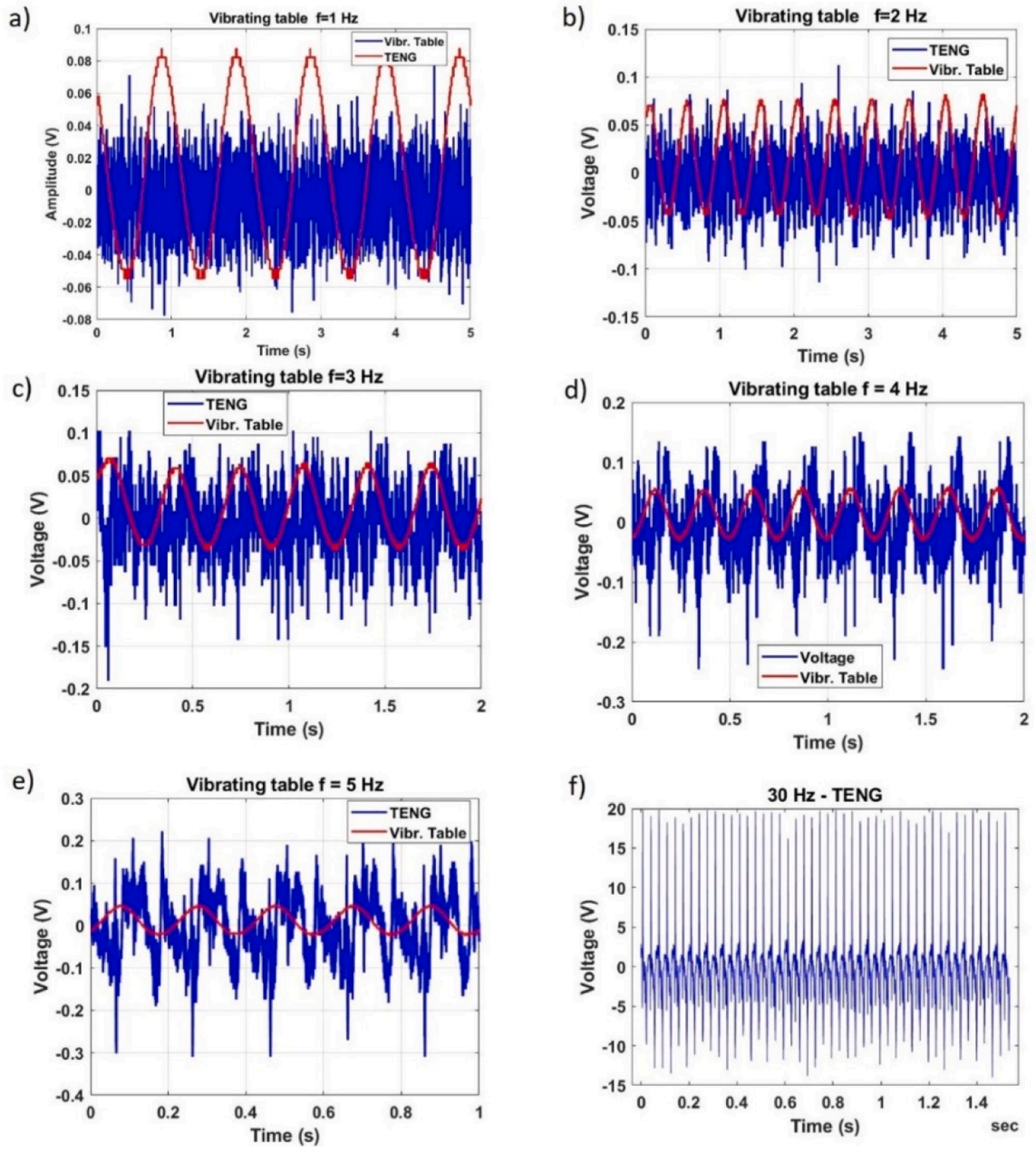

Fig. 8. Voltage generated by the TENG (blue line) for different excitation frequencies (red line) performed with the MASTEC vibrating table and a metal sphere: a) 1 Hz, b) 2 Hz, c) 3 Hz, d) 4 Hz, e) 5 Hz and f) 30 Hz. TENGs presented an initial preload of the sphere in the prism case.

was used to monitor the pulses. In addition, a LABVIEW interface was programmed, and an amplitude threshold was chosen in order to activate a digital output from a low- to an up-state. It is in the up-state when the output digital channel of the NI-DAQ supplies 5 V and a maximum current of 120 mA to a load, such as a light and sound alarm. As reported before, the voltage is related to a value of force according to the force vs. voltage calibration curve and if it was exceeded, the local alarm system would be activated. In addition, another output digital channel would supply a programmed voltage in case another threshold was reached. In this last case, a LoRA MKRWAN1300 emitter, connected to the NI-DAQ output, sent a warning message: "EARTHQUAKE!!", when the vibration amplitude was higher than the threshold programmed meaning the arrival of a high amplitude seismic wave (see Video **SV7** and **SV8**). This message was sent to The Things of Stack (TTS) that is an Internet of Things (IoT) LoRA platform accessible from any device with internet access. In order to send the warning alarm to TTS, a LoRA receiver (RAK2245) sent the data emitted by the MKRWAN1300 to the internet via Wi-Fi and the warning message could be visualized by any user who had internet connection such as a smart phone, PC, smart watch, etc. As the connection emitter-receiver was performed following the LoRA protocol, the distance between them could be around 30 km in areas without any electromagnetic interference (for example, in the countryside with very few antennas). In addition, the program developed in the Arduino IDE can be adaptable and with the aim of ensuring the veracity of the message, the output digital channel would be activated if only more than 5 signals registered presented such a high amplitude.

To finish, a third digital output could change to an up-state in case another threshold programmed in the NI-DAQ was reached. In this situation, a Wi-Fi emitter sent data to activate remotely a receiver that could be placed at a distance up to 2.4 km of distance far away from the emitter. In this case, the receiver supplied electrical power to another visual light and sound alarm and as a result, a warning signal could be

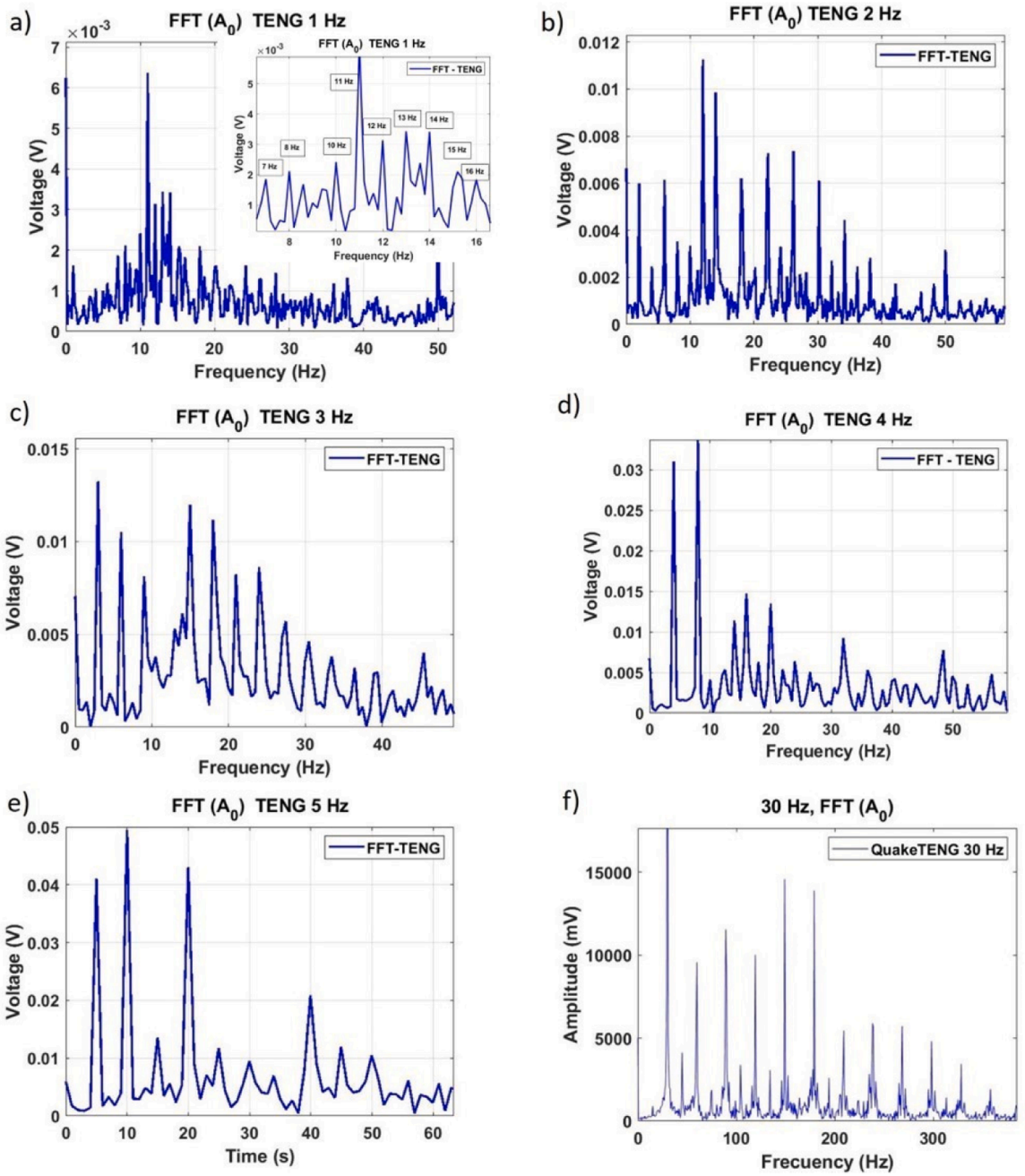

Fig. 9. FFT spectra obtained when applying the FFT algorithm to the TENG voltage signals in the time domain. For a) 1 Hz, b) 2 Hz, c) 3 Hz, d) 4 Hz, e) 5 Hz and f) 30 Hz. TENGs presented an initial preload of the sphere in the prism case.

detected remotely by others, informing about the general state of the ground. Other two output signals were habilitated by the receiver and with the aim of connecting different devices operating with the same or less electrical power than the power supplied by the aforementioned digital output (they were 2 LEDs). The operation of this EDAS can be seen in the videos **SV6-SV8** and Fig. 13. In the video **SV6**, only the light alarm and LEDs are switched on and off remotely via Wi-Fi when the TENG pulse amplitudes are higher or lower respectively than the threshold programmed in LabVIEW. In addition, the videos **SV7** and **SV8** are the same as the video **SV6** but including the MKRWAN1300 and the RAK2245 that allows the communication via LoRA between the emitter (MKRWAN1300) and the receiver (RAK2245) that is connected to the internet and send messages such as EARTHQUAKE!!! via LoRA to the LoRA platforms such as The Things of Sack (TTS). This messages, as reported before, can be read from any device with internet access. In the video **SV7**, a local light alarm (red LED) is included in the previous set-up of the video **SV6** and was connected in the first stage to the NI-USB-600 DAQ: as soon as the TENGs of SLOW-SEISTENG generates voltage pulses higher than the threshold program, the two outputs of the Ni-DAQ will supply the programmed power in the interface to the red LED and as result, the LED will be switched on. Then, the Wi-Fi emitter will be activated so that it will supply power to the light alarm sensors the same as to the input analogue channel of the MKRWAN1300 that is now connected to such receiver. In case the voltage pulse amplitudes are higher than the threshold programmed in the IDE of Arduino, the LoRA gateway MKRWAN1300 will send a message of "GROUND MOTION" to the RAK via Wi-Fi and this one to The Things of Stack (TTS) accessible through internet. This message, as reported above, can be read in anywhere with any type of smart device such as a tablet or cellphone connected to internet.

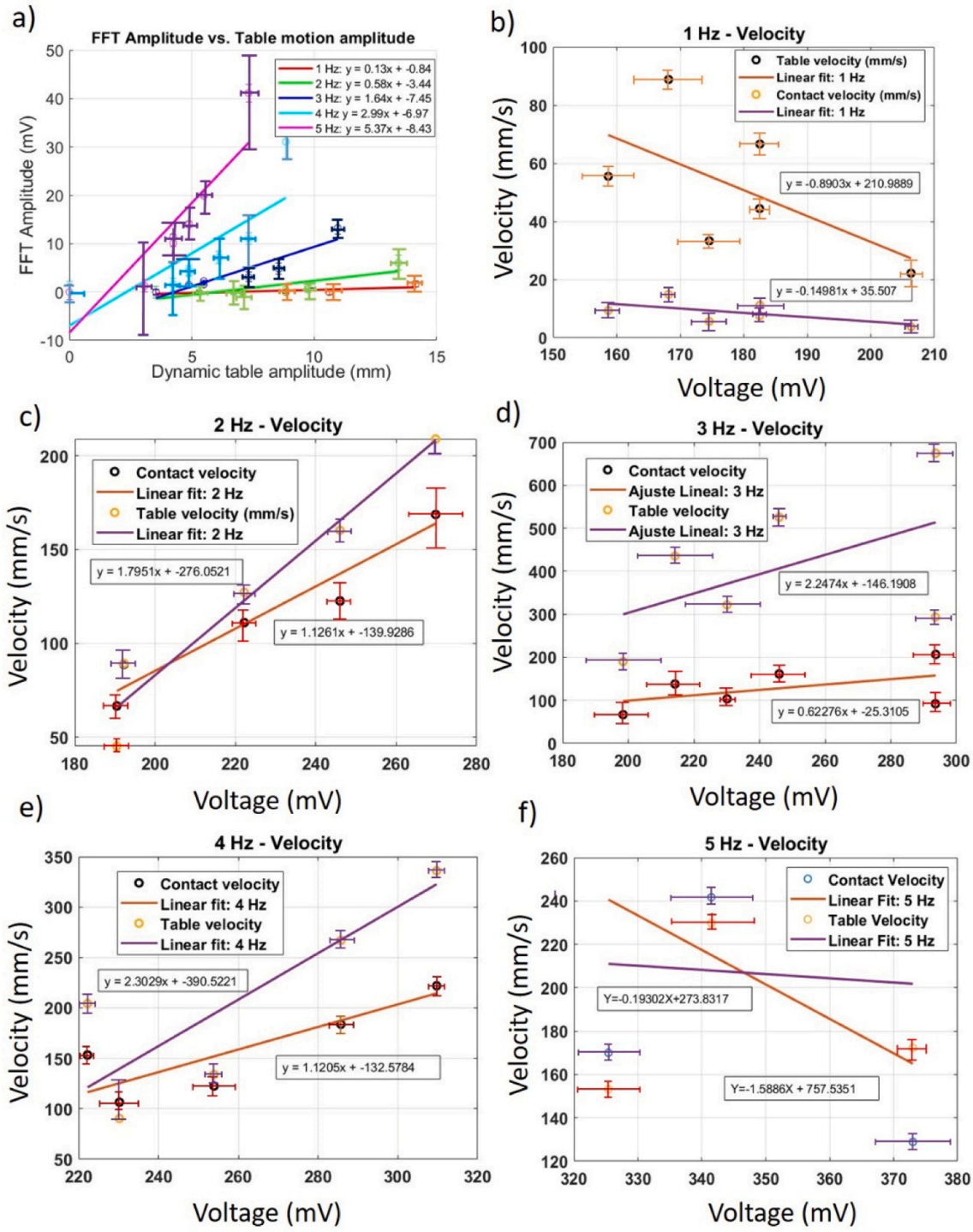

Fig. 10. a) TENG Fast Fourier Transform (FFT) amplitude of the first harmonic vs. elongation experimented by the shake table. TENG peak to peak voltage vs. Velocity of the shake table and wave velocity when the spherical mass is in contact with the TENG for b) 1 Hz of excitation frequency, c) 2 Hz, d) 3 Hz, e) 4 Hz and f) 5 Hz.

In addition, as an example of smart detection, different pulses stored in the memory of a PC were analyzed using machine learning algorithms with the Statistics and Machine Learning toolboxes from Matlab. Two kind of pulses, one coming from the impact supported by the vibration table and named earthquake pulse and the other from a much weaker and shorter impact generated by the vibration of the floor in the street due to a metro arriving to the station, named metro pulse, were classified by using Supporting Vector Machine (SVM) classification algorithm. Features extracted from the pulses are the following: maximum voltage, minimum voltage, pulse width, rise time, fall time and pulse area. Once the algorithm was trained, the SVN classification algorithm was used to predict if 10 pulses generated were coming from either a metro vibration or an earthquake. The results from the program show that two events were from the metro and two from the Earthquake with a 100 % of efficiency. This is shown in Fig. 14 where the two different waveforms (Fig. 14 a)) and the predicted results (Fig. 14 b)-k)) are shown.

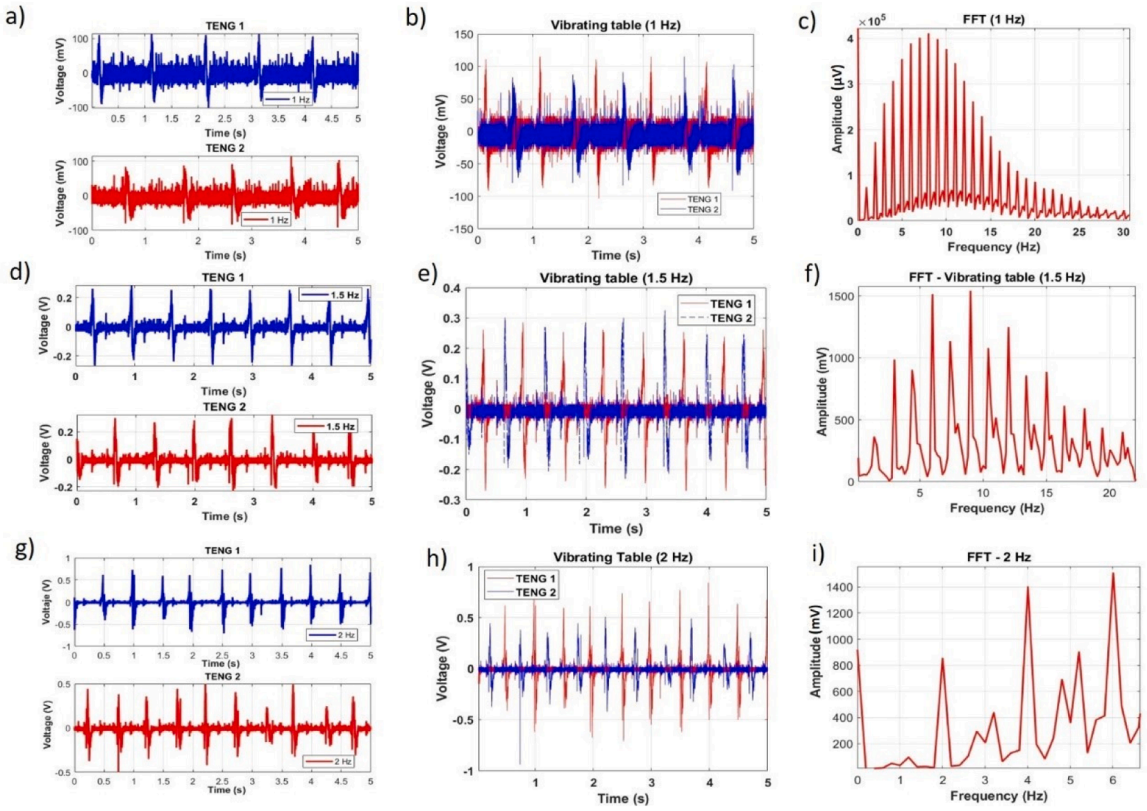

Fig. 11. TENG pulses generated by the inertial mass of the seismic sensor device when there is not any preload for: a) Separated pulses for 1 Hz. B) Pulses together at 1 Hz. C) FFT for 1 Hz. d) Separated pulses for 1.5 Hz. e) Pulses together at 1.5 Hz. f) FFT for 1.5 Hz g) Separated pulses for 2 Hz. h) Pulses together at 2 Hz. i) FFT for 2 Hz. TENGs had not any initial preload of each of the spheres in the prism case.

4. Discussion

This work presents a unique seismic sensor based on the triboelectric energy able to detect slow ground motion (wave velocity of 10 mm/min for forces of fewer than 100 N) the same as higher ones with higher frequencies (velocity of 60 mm/min, F>100 N). As shown in **Fig. S9**, there is a minimum velocity and force when the charge generated is enough to form the pulse, as can be deduced from the conventional triboelectric sensing principle for slow motion. Furthermore, once minimum triboelectric energy to generate a pulse is detected, the duration of the pulse can be as long as needed depending on the time external force (jaws in this work) and the TENG being in contact with them from a minimum force or velocity to higher ones. According to **Fig. S9** and Fig. 5, forces greater than 350 N are necessary to generate a high number of pulses with a well formed waveform for a velocity of 50 mm/min. For the case of 400 N, all pulses presented a characteristic pulse-shape. However, for lower dynamic values an analysis could be performed only in the case of a low band-pass filtering and smoothing functions being applied to raw values. Higher velocities would also contribute to a better formation of the pulse.

Regarding slow-motion detection with TENGs, when measuring low frequencies (often related to small velocities), the formation of the pulses generated by the TENG is significantly dependent on the force magnitude. A minimum velocity and a minimum force are necessary for the sensor to generate electric current. For values lower than 10 mm/min (for F=450 N) and forces lower than 350 N (for v=50 mm/min), it is difficult to detect pulses with the same characteristics (amplitude and waveform) as they are randomly generated by a mechanical external agent (see **Figs. S19–S12**). When higher forces are applied, however, triboelectric energy pulses can be generated for much lower velocities which result in frequency and velocity limits of detection significantly lower than those measured for the tuple (v=50 mm/min, F=350 N) or that of (v=10 mm/min, F=450 N). Thus it could be concluded that PDMS/PVA-based TENGS could operate as low-cost sensors to detect significantly low frequencies and serve as tools used in fields such as geophysics, geology, environmental science and those employed in construction, building edification and risk mitigation.

The calibration curve presented in Fig. 4 a) explains the contribution triboelectric effect has on the electrical energy density in an electrical device. However, the fast spikes measured experimentally and that will conform the pulse when more mechanical or kinematical energy is supplied are very fast (μs) (see Fig. 2) and the instant electrical power produced in the material is not enough to actuate directly on an electronic device, although it could be used as a trigger to initiate an electronic chain. Electrical current generated by the slow motion existing between TENG layers in contact was simulated with the Eq. (1). The representative voltage and current pulse in time obtained from such simulations are shown in Fig. 4 b) and c) respectively. As seen in these figures, velocity between layers substantially increases the triboelectric effect and consequently, the current generated by the TENG and, as a result, the charge. In addition, the most efficient electrical power generated with the TENG is obtained for an electric resistance of 10[41] Ω meaning that it is for this value that a maximum power of 35 μW is delivered to an electronic device with such load (Fig. 4d)). The higher separating distance between layers the lower voltage variation is generated and this is shown in Fig. 4 e) and it is in agreement with the theory describing the electrical field existing between the layers of a plain-parallel capacitor (C=εS/d). This surface electrical potential distribution of the TENG in the XY plane is depicted in Fig. 4 f) for a separating distance between layers of 1 mm and is in agreement with previous figures where the TENG voltage output is plotted.

This study has shown that TENGs are able to detect electromagnetic induction when some conductive material is moving closer to their triboelectric layers. As shown in Fig. 7 a) TENG voltage generated as the

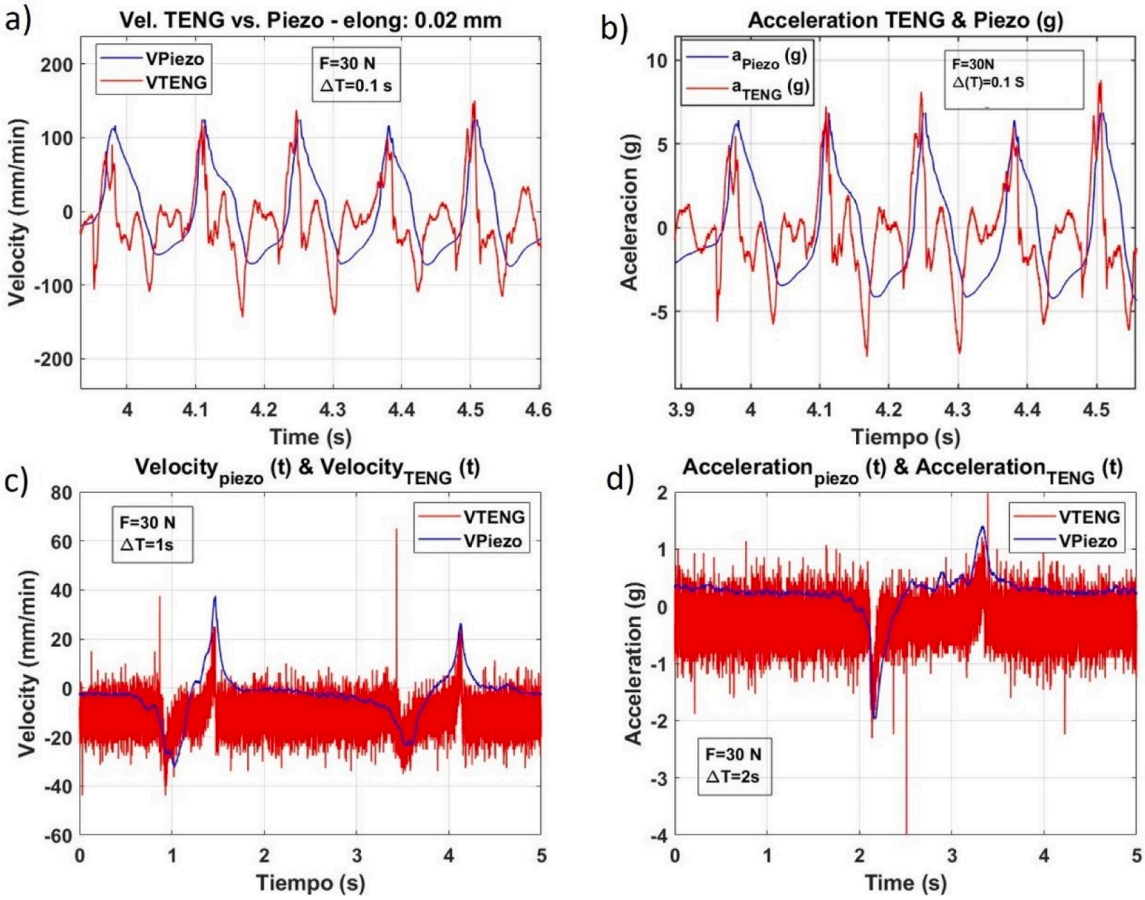

Fig. 12. Comparison between TENG and piezoelectric sensor measurements of: a) Velocity for ΔT=0.1 s; b) Acceleration for ΔT=0.1 s. c) Velocity for ΔT=1 s; d) Acceleration for ΔT=1 s.

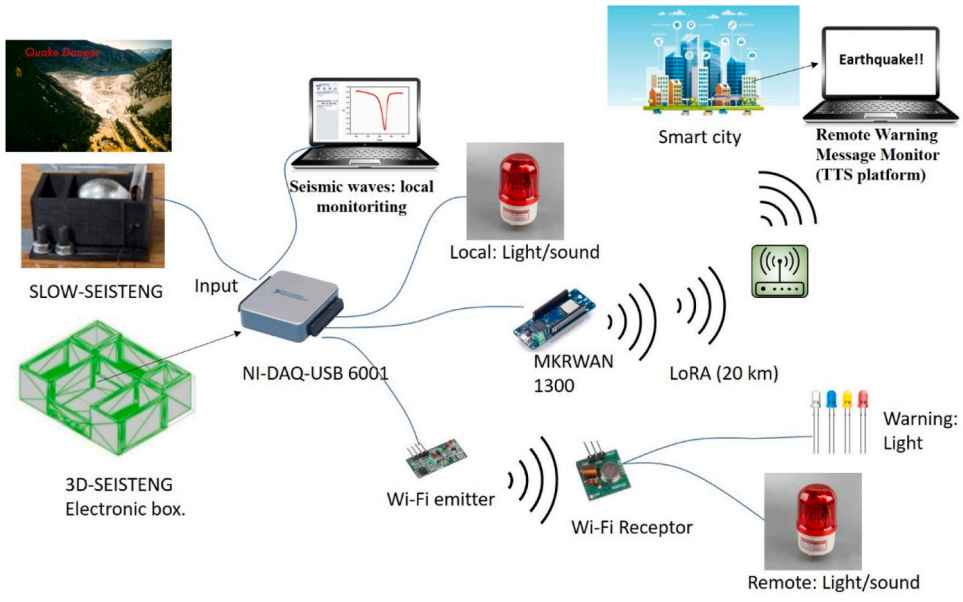

Fig. 13. Sketch of the EDAS (Emergency Detection Alarm system) with SLOW-SEISTENG.

upper jaw sets closer to the TENG (without any contact) is due to the induction of the charged jaws in motion that create a magnetic field which at the same time generates an electromotive force in the TENG, resulting in a small voltage difference between layers and an electric current propagation through the TENG electrodes.

Stability was obtained by leaving the stem operating for some minutes until the voltage baseline monitored in the oscilloscope was constant. However, when no load was applied in the TENG, there was very

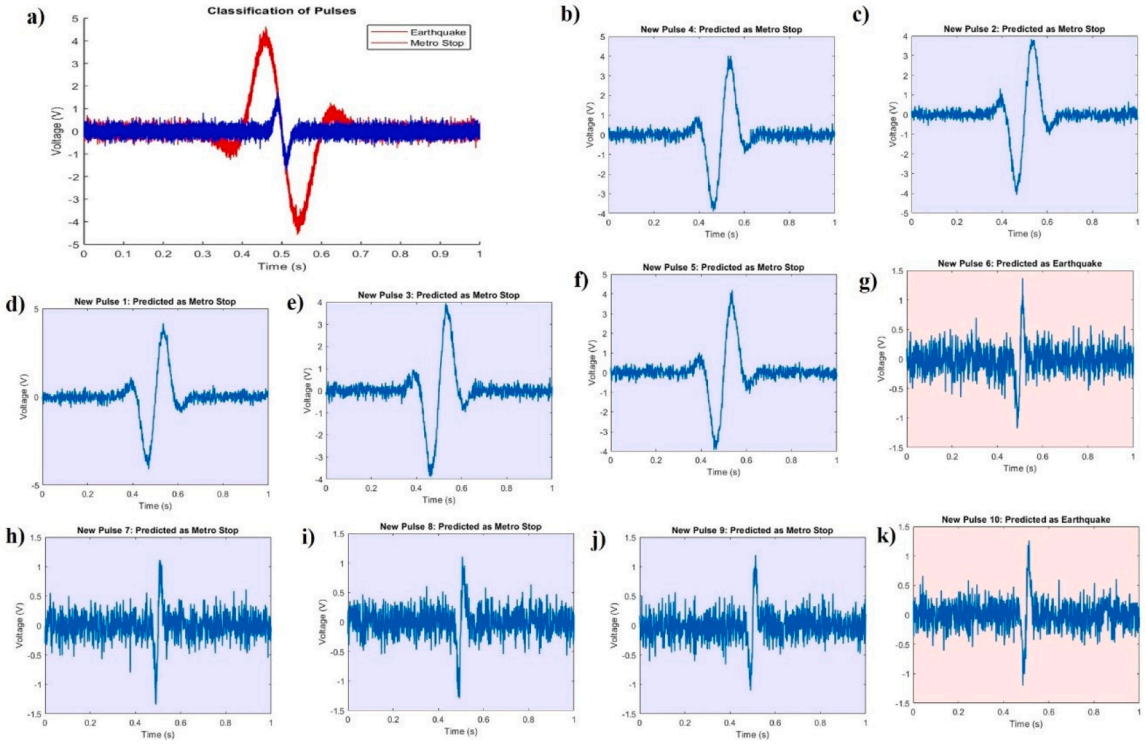

Fig. 14. a) Difference from earthquake and metro pulses. b) First pulse, c) second pulse, d) third pulse, e) fourth pulse, f) fifth pulse, g) sixth pulse h) seventh pulse, i) eighth pulse, j) ninth pulse and k) tenth pulse introduced to be classified as generated by the ground vibration either of a metro or of an earthquake.

little drift and baseline was stable. It is interesting to note that the effect of filtering the TENG voltage signal reduces considerably the signal to noise ratio (SNR). The SNR of the TENG before filtering depends on the TENG and, if it has a preload before beginning the traction/compression cycle, then SNR is higher. Furthermore, SNR velocity of compression/traction is dependent on the frequency cutoff filter. In the case presented in **Fig. S5** a) and b), the SNR before filtering is 138.2 mV and after filtering with a low pass filter of 1 Hz of frequency cut, 69.94 mV (a 50.6 % less). In the case of **Fig. S5** b), the filtered signal has a SNR of 53.23 mV and before filtering, 141.2 mV (a 37.6 % less). The results obtained when FFT was applied to the voltage generated demonstrated the relevance that energy spectra have when analyzing the TENG vibration voltage and displacement due to the motion of the vibration table with the printed box attached on its surface. In Fig. 8 the seismic sensor is operating under a preload where the inertial mass is compressing the sensors. For this reason, voltage generation of TENGs at low frequencies do not give a clear response because force applied to the TENGs is low. This can be seen in Fig. 8 a), b) and c) for the frequencies 1, 2 and 3 Hz. However, in Fig. 8 d) and e) the pulses are clearer shown because of the higher velocity and force applied to the sensors (4 Hz and 5 Hz respectively). The signal is much evident for f=30 Hz where the impact is stronger and velocity and acceleration higher. Interestingly, when applying the FFT to the previous dynamic signals, principal frequencies and their harmonics can be seen in the spectra. In the Fig. 9 a), 1 Hz harmonics are shown. In order to highlight them better, a zoom in the 1 Hz spectrum was performed in the region between 7 and 17 Hz. Furthermore, 2, 3 4, 5 and 30 Hz are well defined in the spectra (Fig. 9 b)-f)).

As can be seen in **2** and **Fig. S15** of SI where impacts are generated as the mass makes contact with the sensors, TENG pulses are well formed even for low frequencies (1 Hz). The pulses plotted either for the dynamic motion (Fig. 11 and **Fig. S15** a) & b, d) & e, g) & h))) or in the Fourier space (Fig. 11 and **Fig. S14**) c), f) & i)) present a much better waveform than when using the system with an initial preload. For low frequencies, the mass follows the whole motion but it seems more difficult to achieve the well-formed pulses, as can be observed in the videos **SV2, SV3** and **SV4**. For 1 Hz, 2 Hz and 3 Hz, the mass follows with high accuracy the table vibration. In addition, a 5 Hz frequency oscillation is shown in the video **SV5** and although is aim mainly due to the surface friction and that the mass is not ideally inertial.

The main concern of using this last configuration of impacts is that it is not as easy to study slow motion as fast events. In addition, using 2 TENGs (each on the opposite walls) enables the study to detect twice the frequency programmed for the vibrating table and demonstrates the capacity TENGs also have to measure fast events. FFT analysis was performed for only one of the sensors, obtaining the same frequencies as the ones programmed in the vibrating table (see Fig. 11 and **video S5)**.

In order to determine the vibration table acceleration and velocity, the piezoelectric D220 allowed obtaining calibration curves of such magnitudes vs. the TENG voltage generated. Calibration curves are shown in the **Fig. S16 b)** and **S18** a) and b). Voltage pulses generated by the piezoelectric sensor for different velocities are plotted in the **Fig. S16** a). A comparison between TENG and piezoelectric sensor measurements of the velocity and acceleration for a time period of the pulse of $\Delta T=0.1$ s and $\Delta T=1$ s are shown in Fig. 12) a) - d). The fact that velocity and acceleration measured with the TENG and the D220 piezoelectric sensor are in agreement with the measurements performed with the INSTRON for different velocities (for a fixed force of F=1 N and an elongation of 0.2 mm) represents the goodness of the seismic sensor calibration curve. This calibration curve could be used to monitor the velocity and acceleration of the seismic waves coming from a simulated earthquake. As this paper shows, the method followed to calibrate the seismic sensors and moreover, its transducers, provides high accurate calibration curves that are essential for different applications. For this reason, a description of these curves and their methods followed is summarized in Section S4. As reported above, a confirmation of the accuracy in the TENG and piezoelectric velocity and acceleration measurements is shown in Fig. 12 a) and b) for excitation periods of $\Delta T=1$ s and in Fig. 12 c) and d) for of $\Delta T=0.1$ s, respectively.

A comparison table of seismic sensors presented in the literature can

be consulted in the supporting information provided by J. Sánchez del Río et al [28]. (see page 18 of the paper). Furthermore, vibration, acceleration, velocity or displacement sensors based on the triboelectric energy nano-generation are also compared in Table 2 according to sensitivity in force, acceleration, velocity and vibration frequency. It can be seen that none of them exhibit the sensitivity sufficiently to measure such low velocity and acceleration values as the ones presented in this paper without any raw signal post-processing or hardware implementation. P. Wang et al. [42] describe an ultra-low-friction triboelectric-electromagnetic hybrid nanogenerator for rotation energy harvesting and self-powered wind speed sensor (ULFHG) operating in freestanding mode and with a rotating electromagnetic generator (EMG), integrated in a solely hybrid energy device. Minimum velocity of the wind of 100 mm/min corresponding to a 1 Hz oscillating frequency was achieved. Q. Zeng et al. [43] described a TENG-based wind energy harvester packaged in a bluff body and connected with a cantilever beam able to measure a minimum wind velocity of 2.8 m/s and a frequency vibration of 3 Hz. Jin Yang et al. [44] fabricated a 3D vibration detector (3D-TENG) based on the triboelectric energy nano-generation and electrostatic induction with the capability of measuring minimum values of 1.2 m/s of velocity, 6 m/s^2 of acceleration, 2.1 Hz of frequency and 0.15 N of force. Gupta et al. [45] presented a polymer-based spring exhibiting multimodal energy harvesting in order to achieve a wide range of accelerations (0.1 *g*-2.0 g) and a low limit of frequency detection of 10 Hz. In addition, velocities of 107 nm/s could be obtained in by G. Zhou et al [46]. with a dynamic motion sensor based on micro-grated triboelectrification and vibration frequencies of 1 Hz and a minimum acceleration value of 0.1 m/s^2 could be measured. A triboelectric self-energy nanogenerator operating as a high sensitive accelerometer is presented by C. Liu et al [47]. and it was able to measure with high accuracy accelerations in the range between 1 and 10 m/s^2. Furthermore, ultra-low frequency mechanical energy detected with TENGs is described by the same previous author Liu C. et al. [16] and frequencies vibration of 0.01 Hz could be obtained after utilizing the modulation of mechanical vibrations. Lastly, the work performed by Hwan Ko et al. [48] depicts vertically grown ZnO nanorod arrays (NRAs) on indium tin oxide (ITO)-coated polyethylene terephthalate (PET), as a top electrode of the nanogenerators. These arrays were investigated for the antireflective property as well as an efficient contact surface in bare polydimethysiloxane (PDMS)-based triboelectric nanogenerators, obtaining 0.25 Hz of frequency vibration for a minimum force of 3 N.

Regarding the applications presented above, the use of SLOW-SEISTENG as an EDAS is relevant for mitigating risks demanded by today's society. The system can be used by either individual citizen in their houses or working offices, by medium and big corporations and governments. The main reason of this general use is because of SLOW-SEISTENG's low-cost, the ease their TENG transducers to be fabricated and the self-energy generation to monitor events. The smart characteristics given to SLOW-SEISTENG by incorporating machine learning algorithms such as supporting vector machines (SVN) to the local data analysis software once seismic information has been stored in different processing units is a key element for its operation either in smart cities or countryside. Although future work will be focused on the evolution of SEISTENG in a more advanced and integrated smart EDAS and more in particular, seismic sensor, the fact that it can operate as part of a much broader network to predict and mitigate risks in different populated areas of the Earth demonstrates the deep impact this system can bring to today's and near future's society.

5. Conclusions

In this work, a unique seismic sensor based on the triboelectric nanogenerators (SLOW SEIS-TENG) is presented. This device is able to detect slow ground motion (wave velocity of 10 mm/min for forces of fewer than 100 N) as well as higher ones with higher frequencies (velocity of 60 mm/s, F>100 N). Notably, motion without contact produced by induction of charges when an inertial mass is moving, which could be measured.

The different calibration curves of velocity, acceleration and force vs. voltage were obtained and could allow operators or controllers to determine earthquake magnitudes and other parameters such as types of pressure waves, possible damage to population and, among others, the epicenter origin. In order to use SLOW-SEISTENG as a high sensitive and reliable sensor, the highest sensitive triboelectric material layers should be chosen to decrease the limit of detection in the different physical magnitudes (force, acceleration, velocity etc.). Once this limit was reached, lower values could be measured but taking into account the stress and strain voltage response of the material chosen. In addition, calibration curves should be performed in the same way as they have been carried out in this work in order to determine its physical response to ground motion.

As a practical use of SLOW-SEISTENG, a realistic alarm system was performed with a LoRA emitter by sending information messages about the earthquake to IoT platforms the same as with Wi-Fi emitters and receivers that allowed activating a sound and visual alarm as soon a threshold programmed and related to the ground motion intensity was exceeded.

In addition, the introduction of machine learning algorithms such as either SVN classification or prediction ones in order to identify the true events makes SLOW-SEISTENG a smart seismic sensor that can be used in the smart cities locally, in citizen houses, offices, warehouses, etc. or remotely, communicating with central point units. In case SLOW-SEISTENG is used in the countryside far away from electromagnetic interferences typically produces in big cities, information regarding the characteristics of the earthquake will be sent more than 20 km far away from the emitter by using LoRA protocol. This makes SLOW-SEISTENG a powerful IoT smart-device that, operating without batteries, could be used to help either individually or the general public to mitigate risks

Table 2
A comparison of different TENG based sensors often used as accelerometers and energy harvesters.

Min. Force (N) (mass in grams (g))	Min. acceleration (m/s^2)	Min. Velocity (m/s)	Min. Frequency (Hz)	Device	Reference
25 N (traction/compr)	2 10^{-5} *	1.6 10^{-4}	0.2	Slow-motion Seismic sensor (TENG)	This manuscript
–	–	3.5	1 Hz	Wind Speed sensor (TENG)	P. Wang et al. [42]
–	–	2.8	3 Hz	Wind energy harvester (TENG)	Q. Zeng et al. [43]
0.15 N (25 g)	6	1.2	2.1	3D vibration detector & energy harvester	Jin Yang et al. [44]
–	0.98	–	10	Electromagn. TENG energy harvester	Gupta et al. [45]
	1x10^{-4}	1.0x 10^{-7}	1	Nanometer resolution micro-grated TENG	G. Zhou et al [46].
0.09 N (10 g/9 m/s^2)	1	–	–	TENG accelerometer	C. Liu et al [47].
			0.01	Ultra-low TENG energy harvester	Liu C. et al. [16]
3N			0.25	PDM-based ZnO nano-rods TENG	Hwan Ko et al. [48]

* The minimum acceleration a_{min} has been calculated in Table 2 by using the following formula: $a_{min} = v/t$. With v the minimum velocity of the inertial mass (in this case the jaws of the INSTROM mechanical machine), 't' the maximum time gap measured and shown in Fig. 3 c) for the minimum acceleration detected, v=10 mm/min and t=8 s. This means that a_{min} =0.02 mm/s^2.

locally or globally.

CRediT authorship contribution statement

José Sánchez del Río: Writing – review & editing, Writing – original draft, Visualization, Validation, Supervision, Software, Resources, Methodology, Investigation, Funding acquisition, Formal analysis, Data curation, Conceptualization. **Antonio Vázquez-López:** Validation, Software, Methodology, Investigation, Formal analysis, Data curation. **Alba López Laguna:** Visualization, Methodology, Investigation, Formal analysis, Data curation. **Martin Andolfi:** Methodology, Investigation, Formal analysis. **Rafael Cascón:** Resources, Project administration, Investigation, Formal analysis, Data curation. **Francisco Santos Olalla:** Resources, Project administration, Conceptualization. **Sofía Paramio:** Methodology, Investigation, Formal analysis. **Yolanda Ballesteros:** Resources, Methodology, Investigation, Formal analysis, Data curation. **Carlos Cruz:** . **Vanesa Martínez:** Software, Resources, Methodology, Data curation. **José Luis Jiménez:** Resources, Methodology, Formal analysis, Data curation. **Xiang Ao:** Visualization, Resources, Methodology, Investigation, Formal analysis. **De-Yi Wang:** Validation, Supervision, Resources, Methodology, Investigation.

Declaration of competing interest

The authors declare that they have no known competing financial interests or personal relationships that could have appeared to influence the work reported in this paper.

Acknowledgments

Authors acknowledge E.T.S. de Ingeniería Industrial (ETSII) for lending the vibration table from the Matest model C278 and to Alfonso Allen-Perkins for his support with Python programming language.

Supplementary materials

Supplementary material associated with this article can be found, in the online version, at doi:10.1016/j.rineng.2025.105845.

Data availability

Data will be made available on request.

References

[1] D.C. Bolton, S. Shreedharan, G.C. McLaskey, J. Rivière, P. Shokouhi, D.T. Trugman, C. Marone, The high-frequency signature of slow and fast laboratory earthquakes, J. Geophys. Res. Solid. Earth. 127 (6) (2022), https://doi.org/10.1029/2022JB024170.

[2] A. Seryi, R. Ruland, B. Baklakov, A. Chupyra, A. Erokhin, M. Kondaurov, A. Medvedko, V. Parkhomchuk, S. Singatulin, E. Shubin, J. Lach, D. Plant, V. Shiltsev, Hydrostatic level system for slow ground motion studies at Fermilab and SLAC, in: Proceedings of the IEEE Particle Accelerator Conference 2, 2001, pp. 1479–1481, https://doi.org/10.1109/pac.2001.986720.

[3] C.R. Soto-Ocampo, J.M. Mera, J.D. Cano-Moreno, J.L. Garcia-Bernardo, Low-cost, high-frequency, data acquisition system for condition monitoring of rotating machinery through vibration analysis-case study, Sensors 20 (12) (2020) 1–19, https://doi.org/10.3390/s20123493.

[4] D. Bradney, S. Evans, M. Chu, P. Clausen, A low-cost, high-speed, multi-channel arduino-based data acquisition system for wind turbine systems, Wind Eng. 44 (5) (2020) 509–518, https://doi.org/10.1177/0309524X19862753.

[5] S.Z. Homayounfar, T.L. Andrew, Wearable sensors for monitoring Human motion: A review on mechanisms, materials, and challenges, SLAS. Technol. 25 (1) (2020) 9–24, https://doi.org/10.1177/2472630319891128.

[6] J. Sánchez del Río Sáez, A. Brunete, F. Santos, D. Patrizi, A. Vázquez-lópez, LoRA smart sensors for IoT fire and ground motion safety, in: IEEE ExPat'23 Conference Proceedings, 2023, pp. 271–274.

[7] J. Knejzlík, Data transmission from seismic stations via network agnes using GSM-GPRS technology, Acta Geodyn. et Geomaterialia 1 (1) (2004) 73–76.

[8] A. Sladen, H. Hébert, On the use of satellite altimetry to infer the earthquake rupture characteristics: application to the 2004 Sumatra event, Geophys. J. Int. 172 (2) (2008) 707–714, https://doi.org/10.1111/j.1365-246X.2007.03669.x.

[9] K. Satake, Advances in Earthquake and tsunami sciences and disaster risk reduction since the 2004 Indian Ocean tsunami, Geosci. Lett. 1 (1) (2014) 1–13, https://doi.org/10.1186/s40562-014-0015-7.

[10] M.G. Bostock, A.M. Thomas, A.M. Rubin, N.I. Christensen, On corner frequencies, attenuation, and low-frequency earthquakes, J. Geophys. Res. Solid. Earth. 122 (1) (2017) 543–557, https://doi.org/10.1002/2016JB013405.

[11] W.B. Frank, E.E. Brodsky, Daily measurement of slow slip from low-frequency earthquakes is consistent with ordinary earthquake scaling, Sci. Adv. 5 (10) (2019) 1–7, https://doi.org/10.1126/sciadv.aaw9386.

[12] A. Chandrasekhar, S. Abdul, V. Vivekananthan, G. Khandelwal, N. Prashant, M. Joseph, Y. Purusothaman, J.Smart Maracas Kim, An innovative triboelectric nanogenerator for Earthquake detection and energy harvesting, Nano Energy 123 (November 2023) (2024) 109379, https://doi.org/10.1016/j.nanoen.2024.109379.

[13] J. Sánchez del Río, A. Yusuf, X. Ao, I.A. Olaizola, L.U. López-Puertas, M. Y. Ballesteros, R. Giannetti, V. Martínez, J.L. Jiménez, J.B.B. Monge, X. Chen, D. Y Wang, High-resolution TENGS for earthquakes ground motion detection, Nano Energy 102 (August) (2022), https://doi.org/10.1016/j.nanoen.2022.107666.

[14] I. Kim, Y. Chae, S. Jo, D. Kim, Levitating oscillator-based triboelectric nanogenerator for harvesting from rotational motion and sensing seismic oscillation, Nano Energy 72 (February) (2020) 104674, https://doi.org/10.1016/j.nanoen.2020.104674.

[15] Xiao, X.; Wang, Q.; Yao, B.; Guo, L.; Zhu, C. Research on low-frequency vibration monitoring sensor based on a cantilever-beam-structured triboelectric nanogenerator. 2023.

[16] C. Liu, N. Zhang, J. Li, L. Dong, T. Wang, Z. Wang, Harvesting ultralow frequency (< 1 Hz) mechanical energy using triboelectric nanogenerator, Nano Energy 65 (July) (2019) 104011, https://doi.org/10.1016/j.nanoen.2019.104011.

[17] Bj, M.; Shi, Y.; Mehamud, I. Machine condition monitoring enabled by broad range vibration frequency detecting triboelectric nano-generator (TENG) -based vibration sensors. 2022, 98 (April). https://doi.org/10.1016/j.nanoen.2022.107292.

[18] X. Li, J. Tao, X. Wang, J. Zhu, C. Pan, Z.L. Wang, Networks of high performance triboelectric nanogenerators based on liquid–Solid interface contact electrification for harvesting low-frequency blue energy, Adv. Energy Mater. 8 (21) (2018) 1800705, https://doi.org/10.1002/AENM.201800705.

[19] L. Jin, J. Tao, R. Bao, L. Sun, C. Pan, Self-powered real-time movement monitoring sensor using triboelectric nanogenerator technology, Sci. Rep. 7 (1) (2017) 1–6, https://doi.org/10.1038/s41598-017-10990-y.

[20] D. Liu, X. Yin, H. Guo, L. Zhou, X. Li, C. Zhang, J. Wang, Z.L Wang, A constant current triboelectric nanogenerator arising from electrostatic breakdown, Sci. Adv. 5 (4) (2019), https://doi.org/10.1126/sciadv.aav6437.

[21] M.E. Tobar, R.Y. Chiao, M. Goryachev, Active electric dipole energy sources: transduction via electric scalar and vector potentials, Sensors 22 (18) (2022) 1–16, https://doi.org/10.3390/s22187029.

[22] Z.L. Wang, On the expanded Maxwell's equations for moving charged Media system – General theory, mathematical solutions and applications in TENG, Materials Today 52 (February) (2022) 348–363, https://doi.org/10.1016/j.mattod.2021.10.027.

[23] Z.L. Wang, On the first principle theory of nanogenerators from Maxwell's equations, Nano Energy 68 (November 2019) (2020) 104272, https://doi.org/10.1016/j.nanoen.2019.104272.

[24] Y. Zi, H. Guo, Z. Wen, M.H. Yeh, C. Hu, Z.L. Wang, Harvesting low-frequency (<5 Hz) irregular mechanical energy: A possible killer application of triboelectric nanogenerator, ACS. Nano 10 (4) (2016) 4797–4805, https://doi.org/10.1021/ACSNANO.6B01569/ASSET/IMAGES/NN-2016-01569S_M016.GIF.

[25] C. Liu, N. Zhang, J. Li, L. Dong, T. Wang, Z. Wang, G. Wang, X. Zhou, J. Zhang, Harvesting ultralow frequency (< 1 Hz) mechanical energy using triboelectric nanogenerator, Nano Energy 65 (2019) 104011, https://doi.org/10.1016/J.NANOEN.2019.104011.

[26] M. Willatzen, Ultrasound transducer modeling-general theory and applications t o Ultrasound, IEEe Trans. Ultrason. Ferroelectr. Freq. Control (2001).

[27] C. Shan, W. He, H. Wu, S. Fu, K. Li, A. Liu, Y. Du, J. Wang, Q. Mu, B. Liu, Y. Xi, C. Hu, Dual mode TENG with self-voltage multiplying circuit for blue energy harvesting and water wave monitoring, Adv. Funct. Mater. 33 (47) (2023) 1–8, https://doi.org/10.1002/adfm.202305768.

[28] J. Sánchez del Río, A. Yusuf, X. Ao, I.A. Olaizola, L.U. López-Puertas, M. Y. Ballesteros, R. Giannetti, V. Martínez, J.L. Jiménez, J.B.B. Monge, X. Chen, D. Y Wang, High-resolution TENGS for earthquakes ground motion detection, Nano Energy 102 (May) (2022), https://doi.org/10.1016/j.nanoen.2022.107666.

[29] Q. Shi, H. Wang, T. He, C. Lee, Self-powered triboelectric inertial sensor ball for IoT and wearable applications, J. Phys. Conf. Ser. (1) (2018) 1052, https://doi.org/10.1088/1742-6596/1052/1/012030.

[30] H. Hong, X. Yang, H. Cui, D. Zheng, H. Wen, R. Huang, L. Liu, J. Duan, Q. Tang, Self-powered Seesaw structured spherical buoys based on a hybrid triboelectric-electromagnetic nanogenerator for Sea surface wireless positioning, Energy Environ. Sci. 15 (2) (2022) 621–632, https://doi.org/10.1039/d1ee02549j.

[31] Q. Ying, J. Wu, C. Liu, Multi-track triboelectric nanogenerator toward omnidirectional ocean wave energy harvesting, Adv. Mater. Technol. 9 (5) (2024) 1–8, https://doi.org/10.1002/admt.202301824.

[32] Uzabakiriho, P.C.; Haider, Z.; Emmanuel, K.; Ahmad, S.; Haleem, A.; Farooq, U.; Uwisengeyimana, J.D.D.; Mbogba, M.K.; Fareed, A.; Memon, K.; Khan, I.; Hu, P.; Zhao, G. High-performance , mechanically and thermally compliant silica-based solid polymer electrolyte for triboelectric nanogenerators application. 2020, No. May. https://doi.org/10.1002/admt.202000303.

[33] PIEZO.COM. *https://piezo.com/collections/piezoelectric-actuators-motors/products/piezoelectric-extending-transducer-d220-a4br-2513xe*. 2020.
[34] S. Niu, Y. Liu, S. Wang, L. Lin, Y.S. Zhou, Y. Hu, Z.L. Wang, Theoretical investigation and structural optimization of single-electrode triboelectric nanogenerators, Adv Funct Mater 24 (22) (2014) 3332–3340, https://doi.org/10.1002/adfm.201303799.
[35] *Matlab*. 2024. https://es.mathworks.com/.
[36] *COMSOL*. https://www.comsol.com/.
[37] Y. Yu, Hengyu Li, X. Zhang, Q. Gao, B. Yang, Z.L. Wang, T. Cheng, Substantially boosting performance of triboelectric nanogenerators via a triboelectrification enhancement effect, Joule 8 (6) (2024) 1855–1868, https://doi.org/10.1016/j.joule.2024.04.013.
[38] M.A. Murti, R. Junior, A.N. Ahmed, A. Elshafie, Earthquake Multi-classification detection based velocity and displacement data filtering using machine learning algorithms, Sci. Rep. 12 (1) (2022) 1–12, https://doi.org/10.1038/s41598-022-25098-1.
[39] H.S. Hwang, S.Y. Hamm, J.Y. Cheong, S.H. Lee, K. Ha, C. Lee, N.C. Woo, S.M. Yun, K.H. Kim, Effective time- and frequency-domain techniques for interpreting seismic precursors in groundwater level fluctuations on Jeju Island, Korea, Sci. Rep. 10 (1) (2020) 1–14, https://doi.org/10.1038/s41598-020-64586-0.
[40] Z. Zhao, J. Chen, X. Liu, Frequency-domain finite-difference elastic wave modeling in the presence of surface topography, Pure Appl. Geophys. 177 (6) (2020) 2821–2839, https://doi.org/10.1007/s00024-019-02402-1.
[41] L. Ren, B. Li, G. Wei, K. Wang, Z. Song, Y. Wei, L. Ren, Qingping Liu, Biology and bioinspiration of soft robotics: actuation, sensing, and system integration, iScience 24 (9) (2021) 103075, https://doi.org/10.1016/j.isci.2021.103075.
[42] P. Wang, L. Pan, J. Wang, M. Xu, G. Dai, H. Zou, K. Dong, Z.L. Wang, An ultra-low-friction triboelectric-electromagnetic hybrid nanogenerator for rotation energy harvesting and self-powered wind speed sensor, ACS. Nano 12 (9) (2018) 9433–9440, https://doi.org/10.1021/acsnano.8b04654.
[43] Q. Zeng, Y. Wu, Q. Tang, W. Liu, J. Wu, Y. Zhang, G. Yin, H. Yang, S. Yuan, D. Tan, C. Hu, X. Wang, A high-efficient breeze energy harvester utilizing a full-packaged triboelectric nanogenerator based on flow-induced vibration, Nano Energy 70 (January) (2020) 104524, https://doi.org/10.1016/j.nanoen.2020.104524.
[44] J. Yang, J. Chen, Y. Yang, H. Zhang, W. Yang, P. Bai, Y. Su, Z.L. Wang, Broadband vibrational energy harvesting based on a triboelectric nanogenerator, Adv. Energy Mater. 4 (6) (2014) 1–9, https://doi.org/10.1002/aenm.201301322.
[45] R.K. Gupta, Q. Shi, L. Dhakar, T. Wang, C.H. Heng, C. Lee, Broadband energy harvester using non-linear polymer spring and electromagnetic/triboelectric hybrid mechanism, Sci. Rep. 7 (January) (2017) 1–13, https://doi.org/10.1038/srep41396.
[46] Y.S. Zhou, G. Zhu, S. Niu, Y. Liu, P. Bai, Q. Jing, Z.L. Wang, Nanometer resolution self-powered static and dynamic motion sensor based on micro-grated triboelectrification, Adv. Mater. 26 (11) (2014) 1719–1724, https://doi.org/10.1002/adma.201304619.
[47] C. Liu, Y. Wang, N. Zhang, X. Yang, Z. Wang, L. Zhao, W. Yang, L. Dong, L. Che, G. Wang, X. Zhou, A self-powered and high sensitivity acceleration sensor with V-Q-a model based on triboelectric nanogenerators (TENGs), Nano Energy 67 (October 2019) (2020) 104228, https://doi.org/10.1016/j.nanoen.2019.104228.
[48] Y.H. Ko, G. Nagaraju, S.H. Lee, J.S. Yu, PDMS-based triboelectric and transparent nanogenerators with ZnO nanorod arrays, ACS Appl. Mater. Interfaces 6 (9) (2014) 6631–6637, https://doi.org/10.1021/am5018072.